

On the origin of the eccentricities of extrasolar planets

Fathi Namouni

CNRS, Observatoire de la Côte d'Azur, BP 4229, 06304 Nice, France

namouni@obs-nice.fr

ABSTRACT

We develop a phenomenological theory that aims to account for the origin of the large eccentricities of extrasolar planets and that of the small eccentricities in the solar system, the preference for apsidal alignment in non-resonant multi-planet systems, and the origin of the similarities in the eccentricity distribution of extra-solar planets and that of spectroscopic binary stars. We show that if a physical process is weakly dependent on the local dynamics of the companion and imparts a small relative acceleration to the star-companion system, the eccentricity of the companion's orbit is excited to large values depending on the direction and duration of acceleration. A natural candidate for such processes are asymmetric stellar jets and star-disk winds. When the acceleration originates from a precessing jet, large eccentricities can be excited by the resonance of the jet's precession frequency with the induced acceleration's excitation frequency even for nearly perpendicular jets. Precession also reduces the eccentricity amplitude far inside the resonance radius. The acceleration's strength is best constrained in multiplanet systems because of the companions' mutual gravitational perturbations, while the acceleration's duration is bounded by the condition that the residual velocity imparted to the star is smaller than the stellar velocity dispersion in the Galaxy. In the outer parts of the star-companion system where the acceleration excitation time is comparable to or smaller than the orbital period, significant radial migration takes place which may have important consequences for the dynamics of the minor body populations in the solar system. The theory is illustrated with the ν Andromedae binary system.

Subject headings: celestial mechanics – planetary systems — stars: mass loss — stars: winds, outflows

1. Introduction

Since the discovery of the first Jupiter-like planet around 51 Pegasi in 1995, the number of extrasolar planets has exceeded 150, some of which reside in 14 multiplanet systems

(Schneider 1996). Extrasolar planetary orbits differ from the solar system’s in two ways: first is their semi-major axis distribution. Planets can orbit their parent stars much closer than the tenth of Mercury’s distance to the Sun. Second, at a median value of $e = 0.27$, their orbital eccentricities are so high that the only solar system analogs are small bodies such as asteroids and Kuiper belt objects whose orbits have been strongly stirred up by the gas giants. These differences are the more puzzling as it has been recognized that the distribution of semi-major axes and eccentricities of extrasolar planets resemble those of spectroscopic binary star systems, a finding that may hint to common formation or excitation mechanisms (Stepinski & Black 2001).

Current theories of planetary formation suggest that Jupiter-like planets form in a disk of gas and dust orbiting a parent star. Producing planets with small semi-major axes is a natural outcome of the transfer of angular momentum between the disk and the planet (Ward & Hahn 2000). The overall effect of this transfer causes the planet’s orbit to shrink around the star. Radial migration can be stopped by the tidal interaction between the planet and the star (Lin et al. 2000) or through photo-evaporation of the disk’s portion exterior to the planet’s orbit and that is responsible for its inward motion (Hollenbach et al. 2000).

The presence of large eccentricities is perhaps the most surprising feature of extrasolar systems as its unexplained origin contrasts with the known ability of the gas disk to force migration. The transfer of angular momentum between the disk and the planet at the locations of their orbital resonances damps the planetary eccentricity so that the natural outcome of this interaction is a planet on a circular orbit (Goldreich & Tremaine 1981). This led to the investigation of other possibilities: secular perturbations by distant companions (Holman et al. 1997; Terquem & Papaloizou 2002), resonant interactions within a multiplanet system (Chiang et al. 2002; Lee & Peale 2002), and encounters of a spatially extended multiplanet system with passing stars (Zakamska & Tremaine 2004). The advantages and drawbacks of these models have been reviewed by Tremaine & Zakamska (2004). The main recurring observation is that these models provide a solution for some specific planetary system. Moreover, they do not explain the apparent uniqueness of the small eccentricities of the solar system’s planets, the occurrence of the largest eccentricities in some multiplanet systems for the outer more massive companions, and the origin of the similarity with spectroscopic binaries. In this regard, it is conceivable to assume that planets formed from a collapsing proto-stellar cloud but this would solve the problem only for the more massive known planets (Papaloizou & Terquem 2001).

In this work, we aim to explain these observations within a single framework. We choose the premise of standard planetary formation theory that the natural outcome of planetesimal accumulation and gas accretion are planets on co-planar circular orbits. To account for the

similarity of the eccentricity distributions of extrasolar planets and spectroscopic binaries, we consider the excitation caused by physical processes that are weakly dependent on the local dynamics of the companion and which can therefore be modeled by an acceleration that does not depend explicitly on the relative position and velocity of the companion. In section 2, we study the general properties of such an acceleration and show that stellar mass loss phenomena such as jets and winds are natural candidates for the excitation process. However, we do not specialize in the case of stellar jets because we prefer to present this theory as a phenomenological one. The reason is twofold: first, the current knowledge of stellar jets and winds both theoretical and observational is not sufficient to issue a definitive verdict on their role in the eccentricity excitation. Second, the dynamical mechanisms that arise because of such accelerations and that lead to eccentricity excitation and apsidal alignment are not concerned directly with the details of jet and wind generation. In section 3, we demonstrate the basic eccentricity excitation mechanism for the simplest finite duration acceleration, one whose direction is constant with respect to the star-companion system. In the remainder of the paper, we consider the various constraints on the basic acceleration model of section 3 set by: the acceleration’s precession (section 4), the radial migration of the companion (section 5), the companion’s orbital stability and the consistency with the host star’s galactic motion (section 6), the secular perturbations from mutual gravitational interactions in multiplanet systems (section 7), and the presence of distant companions (section 8). The application of this theory to the solar system is further discussed in section 8. Section 9 contains concluding remarks.

2. Phenomenology

In this section, we discuss the form of the eccentricity generating processes that would apply equally to planetary and stellar companions. To this end, we seek processes that are weakly dependent on the local orbital dynamics of the companions. By this we mean that the interaction does not depend explicitly on the relative position and relative velocity of the star-companion system. With this in mind, we note that the simplest way to excite the eccentricity of a companion’s orbit is to subject it to a constant acceleration. Stable excitation of the eccentricity is possible if the constant acceleration is smaller than or comparable to the gravitational accelerations between the star and its companions. Writing the perturbing acceleration as $\mathbf{A} = A\mathbf{u}$ where A represents its magnitude and \mathbf{u} is a unit vector, the eccentricity excitation time is proportional to v/A , where v is the keplerian velocity of the companion. This determines two regions around the host star whether the ratio of the excitation time to the orbital period is larger than or comparable to unity. The former is located closer to the star as the excitation time decreases with the relative distance of the

star to the companion. We call this region the secular excitation region as the eccentricity increase builds up slowly after each rotation of the companion around the star. The eccentricity excitation in this case is derived in sections 3 and 4. The outer boundary of the secular excitation region is the sudden excitation region where the excitation time is comparable to or smaller than the orbital period. The dynamics in the sudden excitation region is considered in section 6. With the acceleration magnitudes that we determine below, the observed planetary companions fall into the secular region. Here and if the perturbing acceleration were strictly constant, the corresponding force would be conservative and the eccentricity excitation would simply result in periodic oscillations between the original value, zero, and some maximum value determined by the parameters of each individual system. We would require that A be finite for a duration comparable to or smaller than the oscillation period induced by the acceleration in order to ensure a finite residual eccentricity. In the secular region, the duration is naturally larger than the orbital period of the planet. In the sudden excitation region, the duration of excitation can be comparable to or smaller than the orbital period of distant companions and the outer minor bodies of the planetary system in order to ensure stability (see sections 6 and 8). We can obtain a minimal estimate of the acceleration’s maximal amplitude, A_0 , in the secular region by requiring that the eccentricity excitation time, be shorter than the age of the planetary system $\sim 10^9$ years. This yields: $A_0 > 3 \times 10^{-16}(v/10 \text{ km s}^{-1}) \text{ km s}^{-2}$.

The direction of acceleration, \mathbf{u} , needs to be specified in an inertial frame as the acceleration does not excite the eccentricity of a companion located in the secular region if it is perpendicular to its orbital plane. The knowledge of the current state of the solar system suggests two options: a local one related to the mean orbital plane of the planetary system, and a global one related to the motion of the system in the Galaxy. For the local option, the vector \mathbf{u} is referred to the total angular momentum of the planetary system or the host star’s rotation axis. In the solar system, we would expect \mathbf{u} to be closest to the angular momentum direction because of the small eccentricities of Jupiter and Saturn. The direction of \mathbf{u} can be made independent of the planetary planes if it is referred to the Sun’s rotation axis which is inclined by 6° to Jupiter’s orbital plane normal. On the scale of a planetary system, the simplest way to achieve an acceleration that is weakly dependent on the dynamics of the companion is by stellar and disk mass loss. The global option can be motivated by the galactic configuration of the solar system: the planets’ mean orbital plane is inclined to the Sun’s orbital plane in the Galaxy by the large value of 60 degrees. Jupiter and Saturn have small eccentricities compared to most of the known giant planets that are not located in their parent stars’ tidal zones. The direction of the acceleration can then be tied to that of the star’s motion in the Galaxy with the expectation that the largest eccentricities correspond to the situation where the planetary orbital plane is coincident with the parent star’s galactic

motion plane. The simplest two options for \mathbf{u} are a constant vector that lies in the galactic mid-plane and does not depend on the star’s motion, and a vector directly related to the star’s motion such as its velocity in the Galaxy, \mathbf{v}_g , or the orthogonal thereof $\mathbf{b} \times \mathbf{v}_g$ where \mathbf{b} is a constant vector. On the larger scale of the solar neighborhood, there are no obvious processes that do not depend explicitly on the relative position and relative velocity of the star-companion system and that would excite the companion’s eccentricity.

Jets and star-disk winds are ubiquitous features of star formation and star-disk interaction (Eisloffel et al. 2000; Hartigan et al. 2000) and are natural candidates for the origin of the perturbing acceleration. Inferred mass loss rates for known young T Tauri stars lie in the range $\sim 10^{-8} M_\odot \text{ year}^{-1}$ to $10^{-10} M_\odot \text{ year}^{-1}$ and may be two orders of magnitude larger depending on the way the rate is measured from the luminosity of forbidden lines (Hartigan et al. 1995; Hollenbach 1985; Kwan & Tademaru 1995). The mass loss process needs to be asymmetric with respect to the companion’s orbital plane in order to produce a residual acceleration. Interestingly, a number of bipolar jets from young stars (Hirth et al. 1994; Lavalley et al. 1997) are known to be asymmetric as the velocities of the jet and counter-jet differ by about a factor of 2. Mass loss processes in young stars therefore yield maximal accelerations:

$$A_0 \sim 10^{-13} \left(\frac{\dot{M}}{10^{-8} M_\odot \text{ year}^{-1}} \right) \left(\frac{v_e}{300 \text{ km s}^{-1}} \right) \left(\frac{M_\odot}{M} \right) \text{ km s}^{-2}. \quad (1)$$

where M is the stellar mass and v_e is the outflow’s high velocity component. The implicit proportionality constant depends on the relative mass loss ratios \dot{M} and ejection velocities of the jet and counter-jet.

Integrated over the duration of acceleration, the star acquires a residual velocity that must be smaller than its galactic velocity else the star is ejected. The residual velocity is further bound by the known random component of the stellar motion. In section 8, we further discuss the mass loss rate values after we consider the constraints obtained from the companion’s orbital stability and from the eccentricity excitation of multiplanet systems. Another requirement for stellar and disk mass loss to be efficient in the secular region is that the momentum communicated to the star be inclined with respect to the companion’s orbital plane as it is the component of the acceleration that lies in the companion’s orbital plane that excites the eccentricity. Studies of molecular outflows suggest that some jets precess over timescales from 10^2 to 10^4 years (Davis et al. 1997; Eisloffel et al. 1996; Terquem et al. 1999). As most T Tauri stars are known to be in multiple systems, a possible way to achieve a jet precession is by warping the accreting disk’s plane through the gravitational perturbation of a stellar companion on an inclined orbit (Terquem et al. 1999). This would not imply that jet acceleration may only explain the large eccentricities of planetary companions in binary

systems. We show in sections 6 and 8 that the acceleration may force the outward migration and possibly the ejection of the stellar companion.

In this paper, we do not specialize in a specific acceleration generating process and therefore we do not enter into such specific details as asymmetric jet generation and precession by an accreting circumstellar disk tidally interacting with a stellar binary component. We study the eccentricity excitation by representing the perturbing process by a finite duration acceleration that is independent of the relative position and velocity of the system. In this respect, the application of this theory to the efficiency of stellar jets in exciting eccentricities is phenomenological and yields useful bounds on the star-disk mass loss rate. We point out that the excitation process that is modeled by this acceleration may depend implicitly on the relative position and velocity of the companion. For instance, the accretion that powers the stellar jet is driven by viscosity which can itself be driven by the planetary embryos through the shocking of the pressure waves they launch in the gas disk (Goodman & Rafikov 2001). In this case, the acceleration from the jet will depend implicitly on the companions' local dynamics.

The equation of motion is that of the two-body problem modified as follows:

$$\frac{d\mathbf{v}}{dt} = -\frac{G(m+M)}{|\mathbf{x}|^3}\mathbf{x} + \mathbf{A}(t) \quad (2)$$

where \mathbf{A} is the relative acceleration acting on the star-companion system, \mathbf{x} and \mathbf{v} are the relative position and velocity, M and m are the masses of the star and the companion. The acceleration is finite over a typical duration that we call τ . For simplicity, we choose the amplitude of acceleration to be one of $A_1(t) = A_0 H(t) \exp -t/\tau$ and $A_2(t) = A_0 / \cosh(t - t_0)/\tau$ where $H(t)$ is the Heaviside unit step function and A_0 is the maximum acceleration amplitude. We will use the notation A_0 when we refer to a constant amplitude acceleration. The connection between the perturbing acceleration and the star's random motion in the Galaxy makes the residual velocity, \mathbf{V} , a relevant parameter in the problem; it is defined as:

$$\mathbf{V} = \int_{-\infty}^{+\infty} \mathbf{A}(t) dt. \quad (3)$$

For a constant \mathbf{u} and the two specific forms we use, $V_1 = A_0\tau$ and $V_2 = \pi A_0\tau$. We note that it is likely that the companion is subject to radial migration due for instance to the tidal interaction with the circumstellar disk. The effect of migration on the eccentricity excitation is discussed in section 5 where we modify (2) to account for migration and show that our conclusions about the eccentricity remain valid in the presence of migration. By using equation (2), we also neglect the tidal effect of the Galactic potential; this is justified by the typical sizes of the planetary and stellar systems considered here.

The eccentricity excitation time, v/A_0 , allows us to split the excitation problem into two cases: the first is when the variation of the direction of \mathbf{A} is small on the scale v/A_0 in which case the direction of \mathbf{A} can be held constant to a good approximation. The eccentricity excitation is demonstrated in this case in section 3. The second case is when the direction of \mathbf{A} varies on a timescale comparable or shorter than v/A_0 . This is the general case of precessing jets which is examined in section 4.

3. Eccentricity excitation

Under the effect of a constant-direction acceleration, $\mathbf{A} = A(t)\mathbf{u}$, the variation of specific angular momentum, $\mathbf{h} = \mathbf{x} \times \mathbf{v}$, is $\dot{\mathbf{h}} = \mathbf{x} \times \mathbf{A}$. As \mathbf{u} is constant, only the projection of the angular momentum along the direction of acceleration, $\mathbf{h} \cdot \mathbf{u}$, is conserved. The rate of change of the angular momentum in the direction orthogonal to \mathbf{h} and \mathbf{u} is obtained from $(\mathbf{u} \times \mathbf{h}) \cdot \dot{\mathbf{h}} = A(\mathbf{u} \cdot \mathbf{x})(\mathbf{h} \cdot \mathbf{u})$ and shows that if \mathbf{u} lies in the orbital plane, the orbit does not gain inclination with respect to its initial state. To find the eccentricity and inclination excitation of the companion's orbit in the secular excitation region, we average the equations of motion and in particular the perturbing acceleration over the fast orbital motion of the companion. This is valid because the excitation time and the acceleration's duration are larger than the orbital period of the companion. We can therefore assume that the acceleration is independent of time in deriving the secular equations. A constant acceleration derives from the potential $R = \mathbf{A} \cdot \mathbf{x}$. Its average with respect to the orbital motion is derived in the Appendix and reads:

$$\langle R \rangle = -\frac{3}{2}a \mathbf{A}(t) \cdot \mathbf{e} = -\frac{3}{2}A(t)ae \sin(\varpi - \Omega) \sin I \quad (4)$$

where $\mathbf{e} = \mathbf{v} \times \mathbf{h}/G(m + M) - \mathbf{x}/|\mathbf{x}|$ is the eccentricity vector of magnitude e and a is the orbital semi-major axis. The last expression is obtained by choosing the z -axis along \mathbf{u} ; in this case, ϖ , Ω and I are the longitude of pericenter, the longitude of ascending node and the inclination of \mathbf{h} with respect to \mathbf{u} . The freedom of choosing a vector base in this plane results from the conservation of $\mathbf{h} \cdot \mathbf{u}$ and leads to the appearance of the combination $\omega = \varpi - \Omega$, the argument of pericenter.

The conservation of $\mathbf{u} \cdot \mathbf{h}$ can be written as $\sqrt{1 - e^2} \cos I = \cos I_0$, where I_0 is the initial inclination of the circular orbit, and allows us to reduce the problem to a single degree of freedom with the potential:

$$\langle R \rangle = -\frac{3}{2}Aa \sqrt{\frac{\sin^2 I_0 - e^2}{1 - e^2}} e \sin \omega. \quad (5)$$

The eccentricity and pericenter evolution is obtained from

$$\dot{e} = -\frac{\sqrt{1-e^2}}{na^2 e} \frac{\partial \langle R \rangle}{\partial \omega}, \quad \dot{\omega} = \frac{\sqrt{1-e^2}}{na^2 e} \frac{\partial \langle R \rangle}{\partial e}, \quad (6)$$

where $n = \sqrt{G(M+m)/a^3}$ is the companion's mean motion (Roy 1991). In a conservative system where $A(t) = A_0$ is constant, e and ω follow curves of constant $\langle R \rangle$. There are equilibria at $\omega = \pm 90^\circ$ and $e = \sqrt{2} \sin(I_0/2)$ corresponding to $I = \cos^{-1}(\sqrt{\cos I_0})$. The maximum value of e is $\sin I_0$ and corresponds to the cycle of initially circular orbits. In Figure (1), we show the orbits of the conservative case for an inclination $I_0 = 30^\circ$.

For initially circular orbits, the identity $\langle R \rangle = 0$ leads to $\omega = 0$ or 180° throughout the evolution. The eccentricity equation then reads:

$$\dot{e} = \frac{3A(t)\epsilon}{2na} \sqrt{\sin^2 I_0 - e^2}, \quad (7)$$

where ϵ is the sign of $\cos \omega$ which is set by the requirement that $e \geq 0$. For initially circular orbits, the discontinuous changes of ω between 0 and 180° correspond to the crossing of the plane $I = 0$ during the oscillation of I between $-I_0$ and I_0 ; it is the result of the geometric requirement that $0 \leq I \leq 180^\circ$ in standard keplerian variables. Finally, the eccentricity that is excited by the perturbing acceleration is:

$$e(T) = \left| \sin \left[\frac{3}{2na} \int_{-\infty}^T A(t) dt \right] \sin I_0 \right|. \quad (8)$$

The inclination is obtained from $\cos I = \cos I_0 / \sqrt{1 - e(T)^2}$. In the conservative case, $A(t) = A_0$, e would oscillate between 0 and $\sin I_0$ at the excitation frequency:

$$n_A = \frac{3|A_0|}{na}. \quad (9)$$

Examples of such oscillations that were obtained from the direct integration of the full equations of motion are shown in Figure (2). The agreement between the secular solution and the results numerical integration is perfect and is due to the fact that A is independent of the relative position and velocity. To optimize the excitation of a finite eccentricity from an initially circular state, the duration of acceleration needs to be smaller than half the oscillation period: $\tau < \pi na/3|A_0|$. A less conservative criterion for eccentricity excitation is that the adiabatic condition, $\tau \gg \pi na/3|A_0|$, that would ensure a long term decrease of e to zero is not satisfied. This allows the eccentricity to experience a few oscillations before settling down to a finite value. For multiplanet systems, this situation leads to strong interactions among the companions which can lead to ejections offering a possible explanation for the existence of many extrasolar planetary systems with one large planet. Examples

of eccentricity excitation at three different semi-major axes (i.e. three different excitation frequencies) are shown in Figure 3 for the two forms of the acceleration’s amplitude where τ has been chosen to yield the same residual velocity V and hence the same final eccentricities for each semi-major axis. Figure 3 also illustrates the dependence of the excitation amplitude on the ratio of the duration to the excitation time. We note that because eccentricity excitation in the secular region is a slow process compared to the orbital time, the convolution of the dynamics under the conservative acceleration A_0 with a finite time window has the effect of shutting off the excitation at some eccentricity value depending on the duration.

We conclude that the eccentricity e can be excited up to $\sin I_0$ and is largest if the initial orbital plane contains the direction of acceleration ($I_0 = 90^\circ$). As $\langle R \rangle = 0$ for initially circular orbits, the argument of pericenter, ω , and the longitude of pericenter, Ω , remain at zero. We show in sections 7 and 8 that this forcing of the pericentre to be aligned with the direction of acceleration favors apsidal alignment in multiplanet system. The inclination I decreases from its initial value pushing the orbital plane away from the direction of acceleration. We also note a interesting feature of this model that the final eccentricity increases outward so that in multiplanet systems, the farthest planets may have the largest eccentricities. This is a consequence of the relative strength of the gravitational acceleration and the perturbing acceleration as a function of distance.

4. Precessing accelerations

The inclination of the direction of acceleration \mathbf{u} is crucial to the excitation of eccentricity in the secular region. If the acceleration is due to a stellar jet that precesses, we expect the excitation amplitude to depend on the ratio of the excitation frequency n_A to the precession frequency Ω_A and that resonant forcing is possible when a match occurs, a situation that is likely since n_A is an increasing function of the semi-major axis a . In the following, we solve the conservative excitation problem with precession, that is we choose $\mathbf{A} = A_0 \mathbf{u}(t)$ where \mathbf{u} rotates at the rate Ω_A . For this problem, it is more convenient to derive the eccentricity vector and angular momentum evolution with secular perturbation theory in vector form (Milankovitch 1939) as:

$$\frac{d\mathbf{e}}{dt} = \frac{1}{na^2} \mathbf{k} \times \nabla_{\mathbf{e}} \langle R \rangle + \frac{1}{na^2} \mathbf{e} \times \nabla_{\mathbf{k}} \langle R \rangle, \quad (10)$$

$$\frac{d\mathbf{k}}{dt} = \frac{1}{na^2} \mathbf{k} \times \nabla_{\mathbf{k}} \langle R \rangle + \frac{1}{na^2} \mathbf{e} \times \nabla_{\mathbf{e}} \langle R \rangle, \quad (11)$$

where $\mathbf{k} = \mathbf{h}/\sqrt{G(M+m)a}$ is the non-dimensional angular momentum vector. Using the secular potential (5), these equations reduce to:

$$\frac{d\mathbf{e}}{dt} = -\frac{3A_0}{2na} \mathbf{k} \times \mathbf{u}, \quad \frac{d\mathbf{k}}{dt} = -\frac{3A_0}{2na} \mathbf{e} \times \mathbf{u} \quad (12)$$

$$\frac{d\mathbf{u}}{dt} = \boldsymbol{\Omega}_A \times \mathbf{u}, \quad (13)$$

where $\boldsymbol{\Omega}_A$ is the rotation vector associated with the precessing acceleration. With precession, the constants of motion are given as:

$$-\frac{3A_0}{2na} \mathbf{u} \cdot \mathbf{e} + \boldsymbol{\Omega}_A \cdot \mathbf{k} = C_1, \quad \text{and} \quad -\frac{3A_0}{2na} \mathbf{u} \cdot \mathbf{k} + \boldsymbol{\Omega}_A \cdot \mathbf{e} = C_2. \quad (14)$$

To find the excitation under the precessing acceleration, we introduce the two vectors $\mathbf{k}_\pm = \mathbf{k} \pm \mathbf{e}$ which decouple the equations of motion and yield:

$$\frac{d\mathbf{k}_\pm}{dt} = \pm \frac{3A_0}{2na} \mathbf{u} \times \mathbf{k}_\pm, \quad \text{and} \quad \mathbf{k}_\pm \cdot \left[\boldsymbol{\Omega}_A \mp \frac{3A_0}{2na} \mathbf{u} \right] = C_\pm \quad (15)$$

where $C_\pm = C_1 \pm C_2$. Note that $|\mathbf{k}_\pm| = 1$ is conserved, a consequence of $\mathbf{k} \cdot \mathbf{e} = 0$ and $\mathbf{e}^2 + \mathbf{k}^2 = 1$. We seek a solution for the vectors \mathbf{k}_\pm through their projection on the basis made up of $\boldsymbol{\Omega}_A$, \mathbf{u} , and $\boldsymbol{\Omega}_A \times \mathbf{u}$. Simple algebra shows that $\boldsymbol{\Omega}_A \cdot \mathbf{k}_\pm$ satisfy the equations:

$$\frac{d^2(\boldsymbol{\Omega}_A \cdot \mathbf{k}_\pm)}{dt^2} + [n_A^2/4 + \Omega_A^2 \mp n_A(\boldsymbol{\Omega}_A \cdot \mathbf{u})] (\boldsymbol{\Omega}_A \cdot \mathbf{k}_\pm) = [\Omega_A^2 \mp n_A(\boldsymbol{\Omega}_A \cdot \mathbf{u})/2] C_\pm, \quad (16)$$

which are those of two harmonic oscillators of frequencies n_\pm :

$$n_\pm^2 = n_A^2/4 + \Omega_A^2 \mp n_A(\boldsymbol{\Omega}_A \cdot \mathbf{u}) = (\boldsymbol{\Omega}_A \mp \boldsymbol{\Omega}_k)^2. \quad (17)$$

where $\boldsymbol{\Omega}_k = 3A_0\mathbf{u}/2na$ is the instantaneous rotation vector of \mathbf{k}_+ . The solutions of the previous equations are:

$$\boldsymbol{\Omega}_A \cdot \mathbf{k}_\pm = \frac{[2\Omega_A^2 \mp n_A(\boldsymbol{\Omega}_A \cdot \mathbf{u})] C_\pm}{2n_\pm^2} + K_\pm \cos(n_\pm t + \phi_\pm). \quad (18)$$

where K_\pm and ϕ_\pm are constants to be determined from the initial conditions. The projections on \mathbf{u} are obtained from the constants of motion as:

$$\mp \mathbf{u} \cdot \mathbf{k}_\pm = \frac{[n_A \mp 2(\boldsymbol{\Omega}_A \cdot \mathbf{u})] C_\pm}{2n_\pm^2} - \frac{2K_\pm}{n_A} \cos(n_\pm t + \phi_\pm). \quad (19)$$

The projections along $\boldsymbol{\Omega}_A \times \mathbf{u}$ are found by noting that $(\boldsymbol{\Omega}_A \times \mathbf{u}) \cdot \mathbf{k}_\pm = \pm 2d(\boldsymbol{\Omega}_A \cdot \mathbf{k}_\pm)/dt/n_A$ which lead to:

$$(\boldsymbol{\Omega}_A \times \mathbf{u}) \cdot \mathbf{k}_\pm = \mp \frac{2n_\pm K_\pm}{n_A} \sin(n_\pm t + \phi_\pm). \quad (20)$$

For initially circular orbits that interest us, the integration constants are given by:

$$K_{\pm} \cos \phi_{\pm} = \frac{[n_A^2 \mp 2n_A(\boldsymbol{\Omega}_A \cdot \mathbf{u})] C_1}{4n_{\pm}^2} + \frac{[2n_A(\boldsymbol{\Omega}_A \cdot \mathbf{u}) \mp 4\Omega_A^2] C_2}{4n_{\pm}^2}, \quad (21)$$

$$K_{\pm} \sin \phi_{\pm} = \mp \frac{n_A C_0}{2n_{\pm}}. \quad (22)$$

where C_0 denotes the initial value of $(\boldsymbol{\Omega}_A \times \mathbf{u}) \cdot \mathbf{k}_{\pm}$. The eccentricity and inclination expressions are obtained from $e = \sqrt{(1 - \mathbf{k}_+ \cdot \mathbf{k}_-)/2}$ and $\cos I = \boldsymbol{\Omega}_A \cdot (\mathbf{k}_+ + \mathbf{k}_-)/2\Omega_A\sqrt{1 - e^2}$ (note that the components of \mathbf{k}_{\pm} are not given in an orthogonal basis; to recover $\mathbf{k}_+ \cdot \mathbf{k}_-$ easily, an additional step is needed and consists of writing \mathbf{u} in terms of its invariant part along $\boldsymbol{\Omega}_A$ and its precessing component along the unit vector \mathbf{u}_A as $\mathbf{u} = \sqrt{1 - (\boldsymbol{\Omega}_A \cdot \mathbf{u})^2} \mathbf{u}_A + (\boldsymbol{\Omega}_A \cdot \mathbf{u}) \Omega_A^{-2} \boldsymbol{\Omega}_A$ and substituting it into equations (19) and (20)). This completes the solution of the excitation by a precessing acceleration.

The eccentricity excitation differs from that without precession in three ways: (i) the excitation amplitude depends on the ratio $n_A/2\Omega_A$, (ii) the motion involves two fundamental frequencies n_{\pm} if $\boldsymbol{\Omega}_A$ and \mathbf{u} are not orthogonal, and (iii) large eccentricity excitation becomes accessible at all initial relative inclinations through the resonance $n_A = 2\Omega_A$ where the frequencies n_{\pm} in the denominators of the amplitudes of \mathbf{k}_{\pm} become small.

In the following, we apply these findings to the case of a precessing jet whose rotation vector $\boldsymbol{\Omega}_A$ is parallel to the initial angular momentum vector or equivalently the initial vector \mathbf{k} . The constants of integration are given as: $C_0 = 0$, $C_1 = \Omega_A$ and $C_2 = -n_A \cos(\alpha)/2$ where α is the angle between \mathbf{u} and $\boldsymbol{\Omega}_A$. Denoting by p the frequency ratio $n_A/2\Omega_A$ and using the solution derived above, we find:

$$e^2 = \frac{p^2 \sin^2 \alpha}{4\nu_+^2 \nu_-^2} [2(3 + p^2) - 4(1 + p \cos \alpha) \cos \nu_+ t - 4(1 - p \cos \alpha) \cos \nu_- t + (1 - p^2 + \nu_+ \nu_-) \cos(\nu_+ - \nu_-) t + (1 - p^2 - \nu_+ \nu_-) \cos(\nu_+ + \nu_-) t] \quad (23)$$

$$\cos I = \frac{1}{2\nu_+^2 \nu_-^2 \sqrt{1 - e^2}} [(p^4 - p^2 + 2 + p^2[p^2 - 3] \cos 2\alpha) + p^2 \sin^2 \alpha (p^2 + 1 + 2p \cos \alpha) \cos \nu_+ t + p^2 \sin^2 \alpha (p^2 + 1 - 2p \cos \alpha) \cos \nu_- t] \quad (24)$$

where $\nu_{\pm}^2 = (n_{\pm}/2\Omega_A)^2 = p^2 + 1 \mp 2p \cos \alpha$ and t is normalized by Ω_A ; for definiteness we take $A_0 > 0$ in what follows.

The location where the frequency match, $p = 1$, occurs defines the nominal resonant semi-major axis $a_{\text{res}} = G(M + m)(2\Omega_A/3A_0)^2$. The frequency ratio can be written

as $p = \sqrt{a/a_{\text{res}}}$. We consider the differences introduced by precession in the three regions: far inside resonance ($p \ll 1$), far outside resonance ($p \gg 1$) and the resonance region $p = 1$. Far inside resonance ($p \ll 1$), the jet precesses faster than the eccentricity excitation leading to a reduction of the eccentricity amplitude from $\sin \alpha$ to $2p \sin \alpha$ as $e = p |\sin \alpha| [(3 + \cos[2p \cos(\alpha)t] - 4 \cos[t] \cos[p \cos(\alpha)t])/2]^{1/2}$. Far outside resonance ($p \gg 1$), the jet's precession is slow compared to the eccentricity excitation so that the latter is described by the expressions given in section 3 for a constant-direction acceleration; the inclination, however, is not. The slow precession causes a modulation of the inclination oscillation between 0 and $\sin 2\alpha$ as $\cos I = [\sin^2 \alpha \cos(pt) \cos(\cos[\alpha]t) + \cos^2 \alpha] / [1 - \sin^2 \alpha \sin^2(pt)]^{1/2}$. In the resonance region, the proximity of p to unity increases the denominators of the eccentricity expression (23) which leads to eccentricities close to unity. The width of the region around resonance where large eccentricity values are reached increases with the jet angle α . These features are illustrated in Figures (4) and (5) where we plot the expressions (23) and (24) for two jet angles $\alpha = 1^\circ$ and 30° , an excitation period $2\pi/n_A = 10^4$ years, and the four values of p : 0.05, 0.5, 0.9, 1 and 50. Figure (4) also includes the result of the integration of the full equation of motion (2) and shows that the solution equations are indistinguishable from the unaveraged numerical solution. This agreement results from the fact that the acceleration is independent of the relative motion and the relative velocity. The figures show that the resonance region does not extend far around $p = 1$ for a jet angle $\alpha = 1^\circ$, as the maximal amplitude for $p = 0.9$ is 0.18 while for $\alpha = 30^\circ$ the resonance region is much wider. We note that consistency in the use of the secular potential requires that p is not too small or equivalently that $\Omega_A \ll n$. Numerical integrations of the full equations of motion show that the eccentricity and inclination expressions can be used as long as $\Omega_A < 0.1 n$. Moreover, as the eccentricity excitation time is n_A , no resonant forcing occurs when $\Omega_A = n$ in the secular region ($n_A \ll n$).

Precession-driven resonant excitation therefore provides a possible way to raise the eccentricity even in low jet angle systems. If a companion happens to be at or cross the excitation region, because of disk-driven migration, not only that the eccentricity will grow but the planet leaves the disk as its inclination is excited in phase with the eccentricity. The tidal interaction of the disk with the planet will not prevent the eccentricity excitation if the precession period of the jet, 10^2 to 10^4 years (Davis et al. 1997; Eislöffel et al. 1996; Terquem et al. 1999), is shorter than the viscous time of the disk, 10^5 to 10^6 years (Adams & Lin 1993). Such a situation offers a possible prospect for stopping migration while exciting the eccentricity provided that (i) the disk is stable to the perturbing acceleration and that (ii) the planet's migration time is longer than the excitation time. These results are discussed further after we constrain the magnitude of the perturbing acceleration in section 8.

5. Effect of radial migration on eccentricity excitation

The changes in the orbital semi-major axis a of the companion have so far been neglected because in the secular excitation region where n_A is smaller than the mean motion n , a constant acceleration will produce small periodic oscillations of the semi-major axis with frequency n . It is possible that radial migration occurs indirectly even for an acceleration that is weakly dependent on the local orbital dynamics. Consider for instance the case where acceleration is caused by mass outflow from the star-disk system. The planet’s orbital revolution is determined by the matter content inside its orbit. If the total mass of that content varies over timescales larger than the orbital period the conservation of angular momentum leads to the radial migration of the companion but does not affect its eccentricity (Jeans 1924) leaving initially circular orbits invariant. This conservation leads to the relation $Ma = M_0 a_0$ which in the case of mass loss induces outward migration. To estimate the related migration, we note that the disk’s mass inside the planetary companion’s orbit is at most several percent of M_0 . If all of this mass is ejected from around the star, the companion’s semi-major axis expands by a corresponding several percent showing that in this case migration is not significant.

Disk-companion interactions usually yields an inward radial migration. To find the effect of migration on the eccentricity excitation, we simulate the disk-companion interaction by the addition of a Stokes-type drag $-k\mathbf{v}$ to the equations of motion (2) where k may be a function of time whose characteristic timescale is larger than the orbital period. Simple algebra shows that in the absence of external acceleration, the drag term conserves the modified angular momentum $\eta \mathbf{h}$ where $\eta = \exp \int k dt$. In terms of osculating orbital elements, the previous relation implies that $a(1 - e^2)\eta^2$ is conserved showing that the drag term leads to orbital migration of the companion with respect to the star. The time dependence of k can be interpreted as the mathematical representation of the decay law of a ; for instance, if $a = a_0(t/\tau_a + 1)^{-\alpha}$, then $k = -\alpha(t/\tau_a + 1)^{-1}/2\tau_a$ with $n\tau_a \ll 1$ where τ_a is the migration timescale that depends on the parameters that regulate angular momentum transfer between the companion and the gas disk. A constant k implies an exponential decay of a . When the migration time is larger than the companion’s orbital period, which is usually the case, the average effect of this drag term conserves the orbit’s eccentricity and the planet stays in its initial circular orbit while migrating with respect to the star.

Radial migration would therefore affect the eccentricity excitation only through the variation of the excitation frequency n_A which is where the semi-major axis enters the excitation mechanism. This is illustrated in Figure (6) where we show an example of the excitation of eccentricity during migration. For multiplanet systems, the eccentricity excitation can be affected by the migration significantly because the acceleration has to compete with mutual

planetary perturbations that tend to precess the planetary orbits at rates that may be faster than the acceleration’s excitation frequency.

6. Keplerian boundary and sudden excitation

In order to be stable, a companion’s orbit needs to receive greater acceleration from the star than from the perturbation. This condition delineates the keplerian region around a star as that for which $G(M + m)/r^2 > |A|$. The natural limit for small orbital perturbations is located closer to the star where the frequency n_A becomes comparable to the local mean motion n of the companion. Near this limit, the forced periodic oscillations of the semi-major axis a are reinforced by the eccentricity and acquire large amplitudes. Denoting by a_{kplr} the semi-major axis of the keplerian boundary where $n_A = n$, we obtain an expression for the magnitude of the perturbing acceleration as:

$$|A_0| \simeq 2 \times 10^{-12} \left(\frac{M + m}{M_\odot} \right) \left(\frac{10^3 \text{ AU}}{a_{\text{kplr}}} \right)^2 \text{ km s}^{-2} \quad (25)$$

which for $a_{\text{kplr}} = 10^3 \text{ AU}$ is an order of magnitude larger than the acceleration of the solar system in the Galaxy, the match occurs near $a_{\text{kplr}} = 3000 \text{ AU}$. The excitation period of this acceleration, $T_A = 2\pi/n_A$, is given as:

$$T_A \simeq 10^6 \left(\frac{M + m}{M_\odot} \right)^{\frac{1}{2}} \left(\frac{a_{\text{kplr}}}{10^3 \text{ AU}} \right)^2 \left(\frac{1 \text{ AU}}{a} \right)^{\frac{1}{2}} \text{ years}. \quad (26)$$

When the boundary a_{kplr} of a given acceleration is located beyond 10^4 AU , the Galactic potential’s tide becomes important (Heisler and Tremaine 1986) and must be included to determine the limits of the boundary. In this work, we will be concerned with smaller values of a_{kplr} . To illustrate the motion near the keplerian boundary, we show an example of an escape orbit of a conservative constant-direction acceleration with $a_{\text{kplr}} = 10^2 \text{ AU}$ and an inclination $I_0 = 30^\circ$ (Figures 7 and 8). The orbit’s initial semi-major axis is 68.5 AU . The characteristics of motion are not strictly keplerian as the companion hovers above the star. The semi-major axis shows periodic oscillations around 100 AU with a significant amplitude. These characteristics depend to a certain extent on the direction of acceleration. A study of the types of motion near the boundary is interesting but not central to the problem of the eccentricity excitation. We remark that the escape orbits offer an interesting way to expel planets from around their parent stars or equivalently to disrupt a binary stellar system. If a companion is formed near the keplerian boundary or is pushed out to it by a possibly remaining inner disk that followed photo-evaporation (Hollenbach et al. 2000; Veras & Armitage 2004), it could become unbound. Systems where the acceleration keeps

an approximately constant direction during eccentricity excitation loose companions without a risk of catastrophic encounters with the star if the initial direction of acceleration does not lie in the companion’s orbital plane such as that of Figure (8).

We remark that the value of a_{kplr} corresponds to the innermost location of the stability boundary because the acceleration’s decay decreases n_A and pushes the stability boundary outward. The acceleration’s finite duration may extend the keplerian boundary depending on the ratio of τ to the excitation time at the keplerian boundary of the conservative problem $T_A(a_{\text{kplr}})/2$. When $\tau \geq T_A(a_{\text{kplr}})/2$, orbits beyond a_{kplr} have enough time to acquire sufficient momentum to escape the gravitational pull of the star. When $\tau \leq T_A(a_{\text{kplr}})/2$, the stability region extends beyond a_{kplr} and its boundary is given by the semi-major axis where $\tau \simeq T_A(a_\infty)/2$ which is larger than a_{kplr} since T_A is a decreasing function of the semi-major axis a . Using the expression of T_A and the residual velocity V , $a_\infty \simeq G(M+m)V^{-2}$, the location where the keplerian velocity matches V .

We now determine the features of orbital excitation in the keplerian boundary for an acceleration whose duration, τ , is smaller than the excitation time at the keplerian boundary. We consider the outermost orbits in the sudden excitation region for which the excitation time is very small compared to the orbital time. To these orbits, the sudden excitation imparts a near instantaneous velocity \mathbf{V} . The changes in the orbital elements are found by expressing three conservation relations. First is the conservation of the potential energy as the position \mathbf{x} is left invariant during the excitation. This is written as:

$$\frac{G(M+m)}{|\mathbf{x}|} = \frac{G(M+m)}{2a_i} + \frac{1}{2}v_i^2 = \frac{G(M+m)}{2a_f} + \frac{1}{2}v_f^2, \quad (27)$$

where a_i , a_f , v_i and v_f are the initial and final semi-major axes and velocities of the companion. Eliminating the potential energy term leads to:

$$\frac{G(M+m)}{a_f} = \frac{G(M+m)}{a_i} - 2\mathbf{v}_i \cdot \mathbf{V} - V^2. \quad (28)$$

For an initially circular companion orbit in a coordinate system where the z -axis is chosen along \mathbf{V} (section 3), the previous equation becomes:

$$\frac{1}{a_f} = \frac{1}{a_i} - \frac{2V \sin I_0 \cos \theta}{\sqrt{G(M+m)a_i}} - \frac{V^2}{G(M+m)}, \quad (29)$$

where θ is the longitude of the companion along its orbit, and I_0 is the inclination of the orbital plane with respect to the direction of the residual velocity \mathbf{V} . This equation determines, for a given \mathbf{V} , the final semi-major axis a_f as a function of a_i and θ . We note that a_f can be larger or smaller than a_i because of the inclination term in the energy equation

(29). This leads to an inward or outward migration of the companion. Note that when \mathbf{V} is perpendicular to the initial orbital plane ($I_0 = 0$), migration is always outward.

The second relation is obtained from the conservation of the linear momentum, $\mathbf{v}_f = \mathbf{v}_i + \mathbf{V}$. For initially circular orbits, the projection of the velocity on the position vector yields: $\mathbf{x} \cdot \mathbf{v}_f = \mathbf{x} \cdot \mathbf{V}$. In the cases that we consider below where the companion is initially at the orbit's nodes, $\mathbf{x} \cdot \mathbf{v}_f = 0$ implying the conservation of the pericenter distance $a_f(1 - e_f) = a_i$ if migration is outward and the apocenter distance $a_f(1 + e_f) = a_i$ if migration is inward. This leads to the following relation that is valid at the nodes:

$$e_f = |1 - a_i/a_f|. \quad (30)$$

Elsewhere on the orbit, one needs to express the projections of the linear momentum conservation equation in order to derive the final eccentricity, longitude of pericenter and longitude of ascending node as functions of the longitude θ . The third relation comes from the conservation of the projection of the angular momentum on \mathbf{V} :

$$\sqrt{a_f(1 - e_f^2)} \cos I_f = \sqrt{a_i} \cos I_0, \quad (31)$$

where I_f is the final inclination of the companion. There are three particular initial semi-major axes that characterize migration: first is a_{esc} , the semi-major axis beyond which the companion can escape at certain longitudes. Second is a_{∞} , the semi-major axis beyond which all companions are lost. Third is a_{out} , the semi-major axis beyond which only outward migration occurs. Using equation (29), we find:

$$a_{\text{out}} = \frac{G(M + m)}{V^2} (2 \sin I_0)^2, \quad (32)$$

$$a_{\text{esc}} = \frac{G(M + m)}{V^2} \left(-\sin I_0 + \sqrt{1 + \sin^2 I_0} \right)^2, \quad (33)$$

$$a_{\infty} = \frac{G(M + m)}{V^2} \left(\sin I_0 + \sqrt{1 + \sin^2 I_0} \right)^2. \quad (34)$$

Migration is inward in the longitude range around $\theta = 180^\circ$ defined by:

$$\theta_{\text{rev}}^{\pm} = 180^\circ \pm \cos^{-1} \left| \frac{\sqrt{a_i}}{2V \sin I_0} \right|. \quad (35)$$

Between a_{esc} and a_{∞} , escape occurs in the longitude range around $\theta = 0$ defined by:

$$\theta_{\text{esc}}^{\pm} = \pm \cos^{-1} \left| \frac{a_i^{-1} - V^2/G(M + m)}{2V \sin I_0 / \sqrt{G(M + m)a_i}} \right|. \quad (36)$$

Figure (9) shows the final semi-major axes and eccentricities at two different inclinations $I_0 = 0$ and 20° for an acceleration corresponding to $a_{\text{kplr}} = 300$ AU and a duration $\tau = 500$

years resulting in a residual velocity $V = 0.35 \text{ km s}^{-1}$. The companions were started at the descending node for $I_0 = 20^\circ$ to illustrate inward and outward migration. Also shown in the same figure are the results of the integration of the full equations of motion (2) with the form $A_1(t)$ confirming the validity of the analytic expressions in the outer keplerian boundary. An example of migration with the form A_2 is used for the eccentricity excitation of the ν Andromedae system in section 8.1. The dependence of migration on the orbital longitude is illustrated in Figure (10) for the inclined orbits with $I_0 = 20^\circ$. The migration and excitation near the keplerian boundary offers a possible way to transport minor bodies in the solar system (section 8.2). For planetary companions, the radial migration that results from the interaction with the disk (section 5) has to be added to the migration in the sudden excitation region in order to ascertain the dynamics in the outer keplerian boundary.

The previous study of orbital stability points out similar constraints for the host star that is accelerated in its motion within the Galaxy. Stellar jets for instance modify the star’s velocity but its galactic motion precludes that $|A_0|$ be larger than that the galactic acceleration for an arbitrarily extended time else the star is ejected. The acceleration’s duration, τ , is therefore an important parameter that determines the star’s orbital stability. A limit on τ can be set by requiring that the residual velocity, V , that contributes to the stellar random motion be smaller than the known velocity dispersion, $\langle v_g \rangle$. The condition $V \leq \langle v_g \rangle$ yields:

$$\tau \leq 10^5 \frac{3 \times 10^{-12} \text{ km s}^{-2}}{A_0} \frac{\langle v_g \rangle}{10 \text{ km s}^{-1}} \text{ years}, \quad (37)$$

which in terms of the size of the keplerian boundary is:

$$\tau \lesssim 10^5 \left(\frac{M_\odot}{M + m} \right) \left(\frac{a_{\text{kplr}}}{10^3 \text{ AU}} \right)^2 \frac{\langle v_g \rangle}{10 \text{ km s}^{-1}} \text{ years}, \quad (38)$$

where we used $V \sim A_0 \tau$. For a precessing acceleration, the duration is extended by a factor $1/\cos \alpha$ where α is the jet angle. In addition, the previous estimate is meaningful for a single acceleration event and does not account for an arbitrary time evolution of the angle α .

7. Mutual planetary perturbations

In section 4, we showed that the precession of the perturbing acceleration affects significantly its ability to excite the companion’s eccentricity. This is also true if the acceleration does not precess but the system contains multiple companions. In this case, mutual gravitational interactions cause the eccentricity vectors to precess and possibly to be locked into resonance. We expect for instance that if the precession rates are much faster than the excitation frequencies, the maximum eccentricities will be reduced. To illustrate the effects of

mutual interactions, we model the Jupiter-Saturn system under the influence of a constant direction acceleration using a direct integration of the equations of motion. We assume that the planets formed in initially coplanar circular orbits and that the planetary orbital plane is inclined by 30° with respect to the direction of acceleration. The semi-major axes and masses are taken as $a_J = 5.20$ AU, $a_S = 9.55$ AU, $m_J = 9.55 \times 10^{-4} M_\odot$ and $m_S = 2.86 \times 10^{-4} M_\odot$. The unperturbed eigenfrequencies of the isolated Jupiter-Saturn system are (Murray & Dermott 1999): $9.6 \times 10^{-4} \text{ }^\circ \text{ year}^{-1}$ and $6 \times 10^{-3} \text{ }^\circ \text{ year}^{-1}$ for e and $-7 \times 10^{-3} \text{ }^\circ \text{ year}^{-1}$ for I corresponding to the eigenperiods $T_1 = 375\,000$ years, $T_2 = 60\,000$ years and $T_3 = 51\,000$ years respectively. Note that the eccentricity amplitudes have a period of $1/(1/60\,000 - 1/375\,000) \sim 71\,000$ years and that there is only one inclination eigenmode due to the freedom of choosing a reference plane for Jupiter’s orbit. The evolution associated with mutual planetary perturbations with no external acceleration is depicted in the top panel of Figure (11) where we have ascribed to the two planets their current eccentricities; the eigenfrequencies of the system are independent of e and I if these are small. We assess the effect of mutual perturbation by applying two different acceleration strengths, $A_0 = 2 \times 10^{-12} \text{ km s}^{-2}$ and $A_0 = 2 \times 10^{-14} \text{ km s}^{-2}$, corresponding to the two values $a_{\text{kplr}} = 10^3$ AU and $a_{\text{kplr}} = 10^4$ AU for the location of the keplerian boundary. Taking $a_{\text{kplr}} = 10^3$ AU yields $T_{AJ} = 4.4 \times 10^5$ years, $T_{AS} = 3.2 \times 10^5$ years; a simulation of this configuration is shown in the bottom panel of Figure (11) for which we removed mutual interactions. The case where both mutual interactions and the perturbing acceleration are turned on is shown in Figure (12). The eccentricities of both planets are excited to 0.3 except that Saturn’s is slightly smaller than Jupiter’s. This can be explained by the fact that $T_{AJ} \sim T_1$ which implies a smaller eccentricity reduction for Jupiter. In the case of Saturn, we have $T_{AS} \gg T_2$ which implies a stronger reduction than observed but the gravitational interaction with a more massive Jupiter compensates that effect and forces a larger eccentricity. The dominant eccentricity oscillation period is modified to 2.6×10^5 years. For $a_{\text{kplr}} = 10^4$ AU, $T_{AJ} = 4.4 \times 10^6$ years, $T_{AS} = 3.2 \times 10^6$ years. These timescales are much larger than the unperturbed eigenperiods implying a strong reduction of the excited eccentricities. Figure (13) shows that both eccentricities are smaller than 0.01. The dominant eccentricity oscillation period in this case is modified to 3.6×10^5 years. We can find the minimum strength of the constant-direction acceleration that can excite Jupiter’s eccentricity to its current value 0.05. Numerical integrations yield $a_{\text{kplr}} = 2600$ AU corresponding to $A_0 = 3 \times 10^{-13} \text{ km s}^{-2}$.

We remark that during the eccentricity and inclination excitation, apsidal alignment is maintained with the libration of $\Omega_S - \Omega_J$ and $\omega_S - \omega_J$ around zero. This is the result of the forcing of the pericenters to be aligned with the direction of acceleration that we encountered in the basic two-body problem of section 3. Note however that the inclination oscillation about the direction of acceleration has been largely suppressed. For $a_{\text{kplr}} = 10^3$ AU (Figure

12), the two planets’ inclinations oscillate around 26° with an amplitude of 3° and a mutual inclination of 0.2° . We can use this feature as another constraint on the initial strength of the constant direction force by imposing the current mutual inclination of Jupiter and Saturn of $\sim 1^\circ$. Numerical integrations yield $a_{\text{kplr}} = 590 \text{ AU}$ and $A_0 = 5.7 \times 10^{-12} \text{ km s}^{-2}$ with maximal eccentricities for Jupiter and Saturn of 0.45.

We can obtain an additional constraint on the perturbing constant-direction acceleration by deriving its duration. We do this for the form A_1 with the following simplified configuration: $a_{\text{kplr}} = 590 \text{ AU}$; the eccentricity excitation occurs during the first oscillation cycle; disk driven radial migration is neglected; and Jupiter and Saturn are assumed to have formed at their current locations. In this case, equation (8) leads to:

$$\tau \simeq \sin^{-1} \left(\frac{e_p}{\sin I_0} \right) \frac{T_e}{\pi}, \quad (39)$$

where e_p is the current eccentricity for Jupiter and $T_e \simeq 1.4 \times 10^5$ years is the excitation period obtained with mutual perturbations. For $e_p = 0.05$, $\tau \sim 5000$ years and the residual velocity $V \sim 1 \text{ km s}^{-1}$. The application of the model to the solar system is further discussed in section 8.2. We finally comment that some of the dynamical features that we have shown in this section can be reproduced analytically by applying the Laplace-Lagrange secular perturbation theory at small e and I , and combining its second order secular gravitational potential with the linearized acceleration potential (4) (i.e. substituting I for $\sin I$ in that expression). This would yield the linearized eigenfrequencies and eigenvectors of the system. We do not follow this approach because we are interested in large eccentricities and the possible effects of mean motion resonances and close encounters.

8. Discussion

The eccentricity excitation theory that we have presented is based on the fact that if a star-companion system is subjected to a relative acceleration that is weakly dependent on the local dynamics, large eccentricities can be achieved. The theory has the following parameters:

1. The magnitude of acceleration, A , which determines the excitation frequency of a star-companion system, and the extent of the keplerian region around the main star.
2. The direction of acceleration, \mathbf{u} , (unit vector) with respect to the initial orbital plane which determines the maximum eccentricity of a star-companion system as the projection of \mathbf{u} on the orbital plane.

3. The rotation vector, Ω_A , which describes the acceleration’s precession whose effect on the eccentricity amplitude and resonant excitation is described in section 4.
4. The duration of acceleration, τ , which for a given eccentricity amplitude (larger than required) permits the selection of the final eccentricity value.

When these parameters are specified, the final orbital state of a planetary or stellar companion can be selected. The orbital configurations of star systems with a single companion are easier to explain than those with multiple companions because the absence of additional perturbers relaxes the constraints on the acceleration’s magnitude or equivalently the size of its keplerian boundary a_{kplr} . Since stellar jets and star-disk winds are ubiquitous features of star formation and since we have established that they can be dynamically responsible for the eccentricity excitation, the known similarities and differences of the eccentricity distributions of planetary companions and spectroscopic binaries can be attributed to the similarities and differences of the physical environments that give rise to the accelerating mass loss processes and not directly to the companions’ formation or their dynamical interaction with the gas disk. In this regard, it would be interesting to be able to associate, for stars of a similar spectral type, similar residual velocities that reproduce the observed companion eccentricities.

The excitation theory is built on a minimal assumption that the perturbing acceleration is explicitly independent of the local dynamics –the basic excitation mechanism (section 3) relies on a constant acceleration that is applied for a finite duration. As a result, multiplanet systems as well as planetary systems of binary stars put strong constraints on the acceleration’s parameters. Once these parameters are specified, a single relative acceleration is applied to all companions, planetary and stellar alike, and sets the fundamental excitation frequencies and amplitudes of the system. These frequencies are influenced by the mutual perturbations of the companions as shown in section 7. In particular, the larger the companions’ number, the more constrained the acceleration’s parameters. In section 8.1, we illustrate this situation with the ν Andromedae binary system which contains multiple planets and a distant stellar companion whose observed location strongly constrains the acceleration’s strength. The application of this theory to the known sample of multiplanet systems is beyond the scope of this paper but it is ultimately the best way to ascertain whether the acceleration mechanism is responsible for the eccentricities of extrasolar planets. Two effects need to receive particular attention: the companions’ possible radial migration which changes the fundamental excitation frequencies as seen in section 5, and the companion’s secular perturbations which circulate the eccentricities. Radial migration can be prescribed by the standard disk-planet interaction theories (Ward & Hahn 2000). The effect of secular perturbations may be disentangled by determining for a given multiplanet system the

amplitudes of the secular modes from observed eccentricities and seeking the acceleration parameters that reproduce the amplitudes of the secular modes and not the observed eccentricities. This procedure would be useful for similar mass planets because the instantaneous eccentricities can be different from the individual secular mode amplitudes. The combination of both migration and secular perturbations relaxes some of the constraints on the model because of the additional freedom in the choice of the frequencies of the secular modes. Such an analysis may help elucidate the eccentricity-mass correlations of extra-solar planets. In the following, we further illustrate how to constrain the acceleration mechanism in the case of the ν Andromedae system (section 8.1) and discuss the relevance of these results to the solar system (section 8.2).

8.1. The ν Andromedae binary system

Three planets orbit ν Andromedae (Butler et al. 1997), two of which have their apsides aligned (Rivera & Lissauer 2000; Lissauer & Rivera 2001; Chiang et al. 2001). The most recent observations of this system (Naef et al. 2004) yield the following orbital elements $a_b = 0.059$ AU, $e_b = 0.020$, $\omega_b = 241^\circ$, $m_b = 0.75 m_J$, $a_c = 0.821$ AU, $e_c = 0.185$, $\omega_c = 214^\circ$, $m_c = 2.25 m_J$, $a_d = 2.57$ AU, $e_d = 0.269$, $\omega_d = 247^\circ$, and $m_d = 2.57 m_J$ where the masses are line-of-sight values, the stellar mass is $M = 1.3M_\odot$.

Using the numerical integration of the full equations of motion (2) to model the eccentricity excitation with a constant-direction acceleration applied to the planetary orbits with their current semi-major axes but with initially circular co-planar orbits, we find that mutual planetary perturbations are strong enough to damp the excitation if the acceleration is smaller than $A_0 \sim 10^{-11} \text{km s}^{-2}$. The equivalent keplerian boundary is at $a_{\text{kplr}} \sim 500$ AU. Below this value, the present configuration can be recovered along with the apsidal alignment of the outer two planets. However, the stellar companion to ν Andromedae (Lowrance et al. 2002) puts an additional constraint on the excitation mechanism. At a projected distance of 750 AU, the presence of this $0.2M_\odot$ companion leaves us two options: either the excitation by acceleration is ruled out because the companion lies far outside the keplerian boundary of the weakest possible acceleration that reproduces the planets' eccentricities, or that it was initially inside the boundary and migrated by the sudden excitation that we discussed in section 6. We point out that the projected distance of 750 AU does not translate necessarily into a semi-major axis as the companion's orbit is likely to be eccentric.

To test the second option, we choose an acceleration of the form A_2 with a conservative keplerian boundary at 300 AU corresponding to $A_0 \sim 3 \times 10^{-11} \text{km s}^{-2}$, a duration $\tau = 2000$ years and an equivalent residual velocity $V = 5.6 \text{km s}^{-1}$. The planetary angu-

lar momentum is inclined by 60° with respect to the direction of acceleration. The stellar companion’s initial orbit has a semi-major axis $a = 298$ AU, an eccentricity $e = 0.3$ and an inclination of 10° with respect to the direction of acceleration. At this large semi-major axis, the stellar companion’s perturbation of the planets is negligible; in particular, the eccentricity excitation by the Kozai mechanism (Holman et al. 1997) is not efficient because the corresponding excitation time ($\sim 10^7$ years) is much larger the duration of acceleration and the eccentricity secular frequency of the isolated two-planet system (~ 7000 years). We have chosen such an eccentric and inclined stellar orbit to decouple the problem of eccentricity excitation for the planetary and stellar companions. We find that the acceleration produces a configuration similar to the observed one with stellar orbital elements: $e = 0.5$, $a = 600$ AU, $I = 50^\circ$ (Figure 14). In particular, we remark that the apsidal alignment that is generic in the basic mechanism of section 3 for two bodies is maintained in the v Andromedae system. We also note that only when the acceleration’s strength is near maximum and the keplerian boundary nears 300 AU, does the orbit acquire a larger eccentricity. The numerical integration also confirms the absence of the Kozai eccentricity perturbations in the orbits’ evolution as suggested by the timescale analysis.

The acceleration’s magnitude of $A_0 \sim 3 \times 10^{-11} \text{ km s}^{-2}$ corresponds to a jet-driven mass loss rate $\dot{M} \sim 10^{-6} M_\odot \text{ year}^{-1}$. This value is within the two orders of magnitude uncertainty in mass loss estimation (section 2). However, the inferred rate is a maximal value in time (e.g. Figure 14) and cannot be compared directly to the observed steady state values which are naturally smaller. An additional constraint on the excitation by jet acceleration is that the planet must not lie far inside the resonance location. In terms of the parameters we introduced, the resonant semi-major axis of the precessing jet is given as:

$$a_{\text{res}} \simeq 4 \left(\frac{M_\odot}{M + m} \right) \left(\frac{a_{\text{kplr}}}{10^2 \text{ AU}} \right)^4 \left(\frac{10^4 \text{ years}}{T_{\text{prec}}} \right)^2 \text{ AU}. \quad (40)$$

where $T_{\text{prec}} = 2\pi/\Omega_A$ is the jet’s precession period. This estimate shows that the most efficient accelerating jets precess with periods of 10^4 years or larger. If the precession angle is large as it is the case here, then the large eccentricity region is extended inside the resonant semi-major axis by a sizable factor (e.g. Figure 5 with $\alpha = 30^\circ$). At $a = a_{\text{res}}/100$, maximum amplitude is 0.17 for $\alpha = 60^\circ$. This simple example allows us to conclude that stellar-disk mass loss is a possible process to provide acceleration. Further modeling of jet acceleration with a more realistic amplitude time variation is needed to constrain the excitation mechanism.

8.2. The solar system

The solar system was used in our model to motivate the possible options of the direction of acceleration using the small eccentricities of Jupiter and Saturn. The detailed analysis of the excitation by acceleration pointed out other ways to limit the eccentricity growth: to the maximum eccentricity set by the inclination of the acceleration with respect to the orbital plane, we add the amplitude reduction associated with a precessing acceleration and that associated with a weak acceleration ($a_{\text{kplr}} > 2600$ AU with $I_0 = 30^\circ$ constant) that competes with mutual planetary perturbations. These options show that it is more difficult to identify the evolutionary track of low eccentricity systems. Modeling the migration of the solar system’s planets and its effects on minor bodies under a perturbing acceleration may offer a way to discriminate between the available options. The current state of the giant planets’ orbits is believed to have evolved from a much more compact system. Studies of the origin of the eccentricity and inclination distributions of Kuiper belt objects suggest that the four giant planets were confined between 5.5 AU and 13.5 AU at the time where the Kuiper belt was made up of a low eccentricity and inclination planetesimal disk (Malhotra 1995; Gomes 2003). For such compact configurations, mean motion resonance crossing may produce eccentricities comparable to the current values for Jupiter and Saturn (Tsiganis et al. 2004). Regardless of the specifics of such mechanisms and if we admit that accelerating processes of the type studied here excited companion eccentricities for solar-type stars in the solar neighborhood, the same processes must have applied to the solar system and shaped it to a certain extent. In the context of acceleration by stellar jets and star-disk winds, the inclination of Jupiter’s angular momentum vector by 6° with respect to the Sun’s rotation axis is an indication that Jupiter’s orbital plane has had to evolve from an equatorial accretion disk or that the planet had formed in a warped disk. Both possibilities are favorable to the excitation by acceleration model.

An interesting application of our model that does not require modifying the standard picture of how the solar system and its minor body populations have evolved is to choose the direction of acceleration nearly perpendicular to the planetary orbital plane. The acceleration, however, may not be particularly weak thereby allowing smaller values of a_{kplr} . The main consequence of such an acceleration is to excite the eccentricities of bodies that lie near the keplerian boundary, eject those that lie far outside it, thus truncating the planetesimal disk, and outward transport those in its vicinity through the migration that we discussed in section 6 and illustrated in Figures (9) and (10). Migration could enhance the delivery of minor bodies to the Oort Cloud and explain the transport of Kuiper Belt outliers 2000 CR105 and Sedna (90377) that, with perihelia larger than Neptune’s semi-major axis, still elude dynamical explanation (Brown et al. 2004; Morbidelli & Levison 2004).

9. Concluding remarks

In this paper, we have worked towards building a theory for the origin of the eccentricities of extrasolar planets. Proceeding with minimal assumptions, we showed that the planetary eccentricities can be caused by relative accelerations that depend weakly on the local dynamics. We have thus reduced the problem of the origin of eccentricities to the identification of the physical processes that cause such accelerations. Possible processes are stellar jets and star-disk winds that accelerate the host star with respect to the companion and excite the random component of its galactic velocity. The origin of extrasolar eccentricities can therefore be related to the the random motion of disk stars in the Galaxy.

The model has further applications to the dynamics of extrasolar planets and the solar system. If the duration of acceleration is larger than the excitation time at some semi-major axis, planets exterior to this radius will achieve maximum eccentricity and risk ejections by close encounters (section 3). This offers a possible explanation for single planet systems with large eccentricities. Rogue planets can also be produced if planets are pushed out to the keplerian boundary by disk-planet interaction (section 6). For the solar system, besides the possible eccentricity excitation, acceleration leads to the transport of minor bodies to the outer Kuiper Belt and the Oort Cloud.

The excitation by acceleration model can be applied in other contexts beside the stellar and planetary and companions. The star-disk mass loss mechanisms, that can be responsible for the eccentricity of extrasolar planets, impart an equal acceleration to the protoplanetary disk. A precessing acceleration derives from the perturbing potential $R = \mathbf{A} \cdot \mathbf{x} = r A_r \cos(\theta - \theta_A) + z A_z$ where θ_A , A_r , A_z are the acceleration's components in a cylindrical coordinate system referred to the disk. This potential could be able to excite the $m = 1$ slow modes of the disk (Tremaine 2001). Such modes are interesting because of their large wavelength that can be comparable to the size of the system. For instance, the disk could develop rigid precession if the speed of sound waves is larger than the precession rate similarly to the case of tilted disks perturbed by a binary component (Papaloizou & Terquem 1995). The feedback of a jet-generated precessing acceleration on the disk may have important consequences for sustaining the acceleration.

The excitation mechanism also applies to galactic dynamics. Large-scale wind phenomena (Bland-Hawthorn & Cohen 2003; Shopbell & Bland-Hawthorn 1998) accelerate the Galaxy and alter the galactic rotation curve by decreasing the circular velocity. The analysis of this paper can be modified to ascertain the efficiency of galactic winds in the excitation of the stellar random motion by substituting the galactic potential for the stellar potential in equation (2). Further applications of galactic winds include the stability of large scale structures in disk galaxies, the onset of $m = 1$ elliptic distortions, and the effect of the

change in the Sun’s Hill sphere in the Galaxy on the dynamics of the Oort Cloud.

Acknowledgments

I thank an anonymous referee for the careful review of the paper and Rodney Gomes, François Mignard and Kleomenis Tsiganis for discussions. This work was supported by the Programme National de Planétologie.

A. Averaged potential of a constant acceleration

In the following, we derive the averaged potential of a constant acceleration \mathbf{A} . The acceleration (or equivalently its force) derives from the potential $R = \mathbf{A} \cdot \mathbf{x}$ where \mathbf{x} is the position vector. The averaged potential is $\langle R \rangle = \mathbf{A} \cdot \langle \mathbf{x} \rangle$ and therefore only the average of the position vector \mathbf{x} needs to be calculated. The companion’s unperturbed orbit is keplerian and in an orthonormal basis can be written as:

$$x = r (\cos \Omega \cos(\omega + f) - \sin \Omega \sin(\omega + f) \cos I), \quad (\text{A1})$$

$$y = r (\sin \Omega \cos(\omega + f) + \cos \Omega \sin(\omega + f) \cos I), \quad (\text{A2})$$

$$z = r \sin(\omega + f) \sin I, \quad (\text{A3})$$

where the radius is $r = a(1 - e^2)/(1 + e \cos f)$ and the orbital elements a , f , e , ω , I , and Ω are respectively, the semi-major axis, the true anomaly, the eccentricity, the argument of pericenter, the inclination and the longitude of the ascending node. The time average can be replaced with a true anomaly average by using the conservation of angular momentum $dt/P = r^2 df / 2\pi a^2 \sqrt{1 - e^2}$, where P is the period. Applying this integration to the position vector gives:

$$\langle \mathbf{x} \rangle = -\frac{3}{2} a e \frac{\mathbf{x}}{r}(f = 0). \quad (\text{A4})$$

The direction of \mathbf{x} at $f = 0$ is that of the eccentricity vector (or Runge-Lenz vector), $\mathbf{e} = \mathbf{v} \times \mathbf{h}/G(M + m) - \mathbf{x}/r$. The averaged potential is therefore:

$$\langle R \rangle = -\frac{3}{2} a \mathbf{A} \cdot \mathbf{e}. \quad (\text{A5})$$

Inspection of the position vector equations shows that the simplest expression corresponds to choosing the z -axis as the direction of acceleration. This leads to $\langle R \rangle = -3aeA \sin(\varpi - \Omega) \sin I/2$ where $\varpi = \omega + \Omega$ is the longitude of the pericenter, the conjugate variable of the eccentricity, e .

REFERENCES

- Adams F.C., Lin D.N.C., 1993. In *Protostars and Planets III*. pp 721. University of Arizona Press. Eds: E.H. Levy, Lunine J.I.
- Brown M.E., Trujillo C., Rabinowitz D., *ApJ*, 2004, 617, 645
- Bland-Hawthorn J., Cohen M., 2003, *ApJ*, 528, 246
- Butler R.P., Marcy G.W., Williams E., Hauser H., Shirts P., 1997, *ApJL*, 474, L115
- Chiang E.I., Tabachnik S., Tremaine S., 2001, *AJ*, 122, 1607
- Chiang E.I., Fischer D., Thommes E., 2002, *ApJ*, 564, L105
- Davis C.J., Eislöffel J., Ray T.P., Jenness T., 1997, *AA*, 324, 1013
- Eislöffel J., Smith M.D., Davis C.J., Ray T.P., 1996, *AJ*, 112, 2086
- Eislöffel J., Mundt R., Ray T.P., Rodríguez L.F., 2000. In *Protostars and Planets IV*. pp 815. University of Arizona Press. Eds: Mannings V., Boss A. P. and Russel S. S.
- Goldreich P., Tremaine S., 1981, *ApJ*, 243, 1062
- Gomes R., 2003, *Icarus*, 161, 404
- Goodman J. and Rafikov R., 2001, *ApJ*, 552, 793
- Hartigan P., Edwards S., Pierson R., 1995, *ApJ* 452, 736
- Hartigan P., Mundt J., Reipurth B., Morse J.A., 2000. In *Protostars and Planets IV*. pp 841. University of Arizona Press. Eds: Mannings V., Boss A. P. and Russel S. S.
- Heisler J., Tremaine S., 1986, *Icarus* 65, 13
- Hirth G.A., Mundt R., Solf J., 1994, *ApJ*, 427, L99
- Hollenbach D., 1985, *Icarus*, 61, 36
- Hollenbach D.J., Yorke H.W., Johnstone D., 2000, In *Protostars and Planets IV*. pp 401. University of Arizona Press. Eds: Mannings V., Boss A. P. and Russel S. S.
- Holman M., Touma J., Tremaine S., 1997, *Nature*, 386, 254
- Jeans, J. 1924, *MNRAS*, 84, 2

- Kwan J., Tademaru E., 1995, ApJ, 454,382
- Lavalley C., Cabarit S., Dougados C., Ferruit P., Bacon, R., 1997, AA, 327, 671
- Lee M.H., Peale S.J., 2002 ApJ, 567, 596
- Lin D.N.C., Papaloizou J.C.B., Terquem C., Bryden G., Ida S., 2000, In Protostars and Planets IV. pp 1111. University of Arizona Press. Eds: Mannings V., Boss A.P. and Russel S.S.
- Lissauer J.J., Rivera E.J., 2001, ApJ, 554, 1141
- Lowrance P.J., Kirkpatrick J.D., Beichman C.A., 2002 ApJ, 572, L79
- Malhotra R., AJ, 110, 420
- Milankovitch M, 1939. Bull. Acad. Math. Natur. (A) Sci. Math. Phys. number 6. Belgrade.
- Morbidelli A., Levison H.F, 2004, AJ, 128, 2564
- Murray C.D., Dermott S.F., 1999, Solar System Dynamics. Cambridge University Press.
- Naef D., Mayor M., Beuzit J.L., Perrier C., Queloz D., Sivan J.P., Udry, S., 2004, AA, 414, 351
- Papaloizou J.C.B., Terquem C. 1995, MNRAS, 274, 987
- Papaloizou J.C.B., Terquem C. 2001. MNRAS 325, 221
- Rivera E.J., Lissauer J.J., 2000, ApJ, 530, 454
- Roy A. 1991, Orbital motion. Adam Hilger, Bristol.
- Schneider J. 1996. <http://www.obspm.fr/planets>
- Shopbell P.L., Bland-Hawthorn J., 1998, ApJ, 493, 129
- Stepinski T.F., Black D.C., 2001, A& A 371, 250
- Terquem C., Eislöffel, Papaloizou J.C.B., Nelson R.P., 1999, ApJ, 512, L131
- Terquem C., Papaloizou J.C.B., 2002, MNRAS, 332, L39
- Tremaine S., 2001, AJ, 121, 1776

Tremaine S., Zakamska N., 2004. AIP Conf. Proc. v. 713, pp 243. Eds. S.S. Holt and D. Deming

Tsiganis, K., Morbidelli A., Levison H.F., Gomes R.S., 2004, BAAS, 36, 44.08

Veras D., Armitage P.J., 2004, MNRAS, 347, 613

Ward W.R., Hahn J.M., 2000. In Protostars and Planets IV. pp 1135. University of Arizona Press. Eds: Mannings V., Boss A. P. and Russel S. S.

Zakamska N., Tremaine S., 2004, AJ, 128, 869

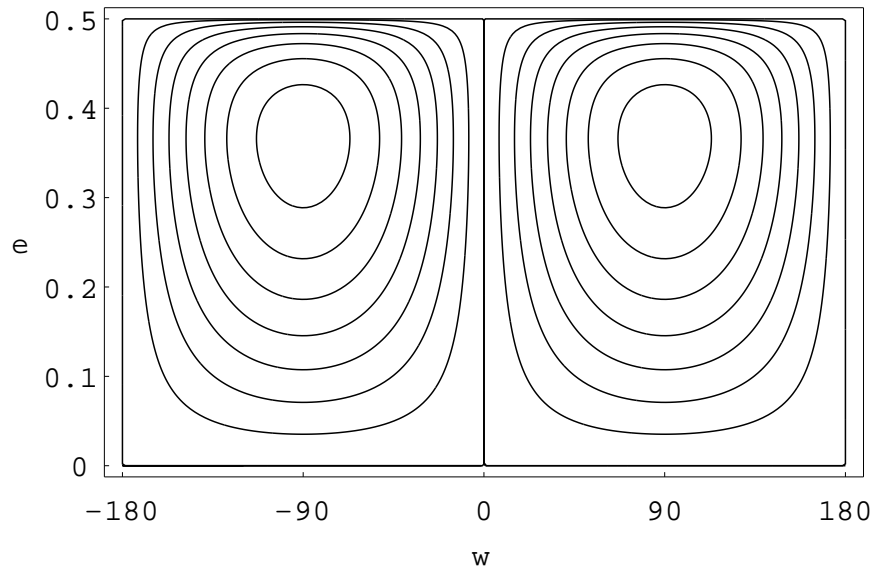


Fig. 1.— Contour plots of the acceleration potential (5) in the eccentricity e and argument of pericenter $\omega(^{\circ})$ plane. The direction of acceleration makes an angle $I_0 = 30^{\circ}$ with respect to the companion’s angular momentum vector. The time evolution of the two orbits ($e = 0$, $\omega = 0$) and ($e = 0.3$, $\omega = 90^{\circ}$) is shown in Figure (2).

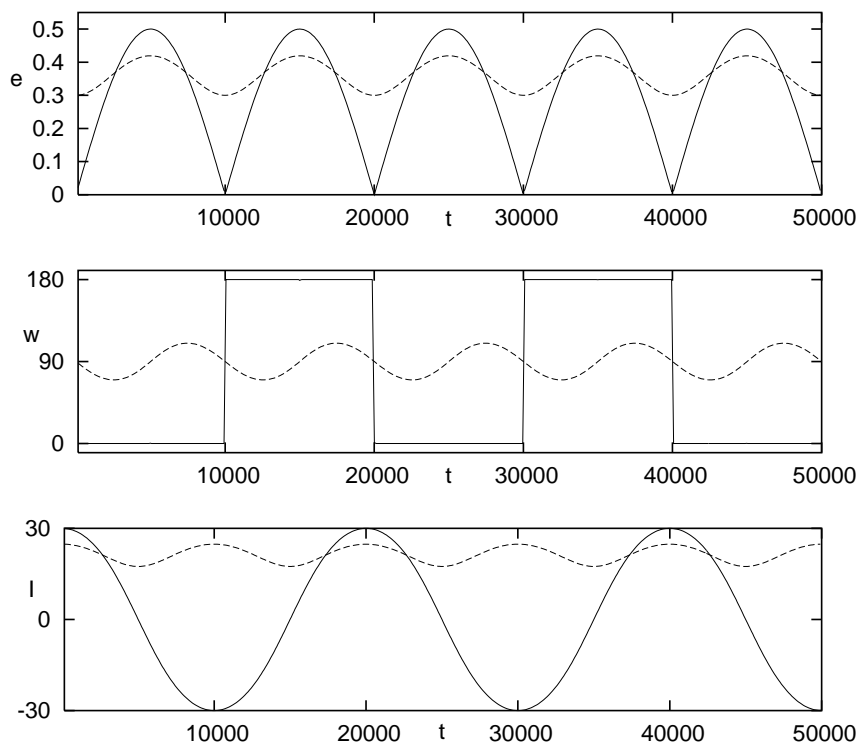


Fig. 2.— Time evolution under a conservative acceleration. The eccentricity e , argument of pericenter $\omega(^{\circ})$ and inclination $I(^{\circ})$ are shown for an initially circular orbit $e = 0$ (solid) and an orbit librating about the secular resonance $\omega = 90^{\circ}$ with an initial eccentricity $e = 0.3$ (dashed). The semi-major axis is identical for both orbits and is set to unity. The acceleration corresponds to a period of 10^4 years at 1 AU. The plots were obtained by the numerical integration of the full equations of motion (2).

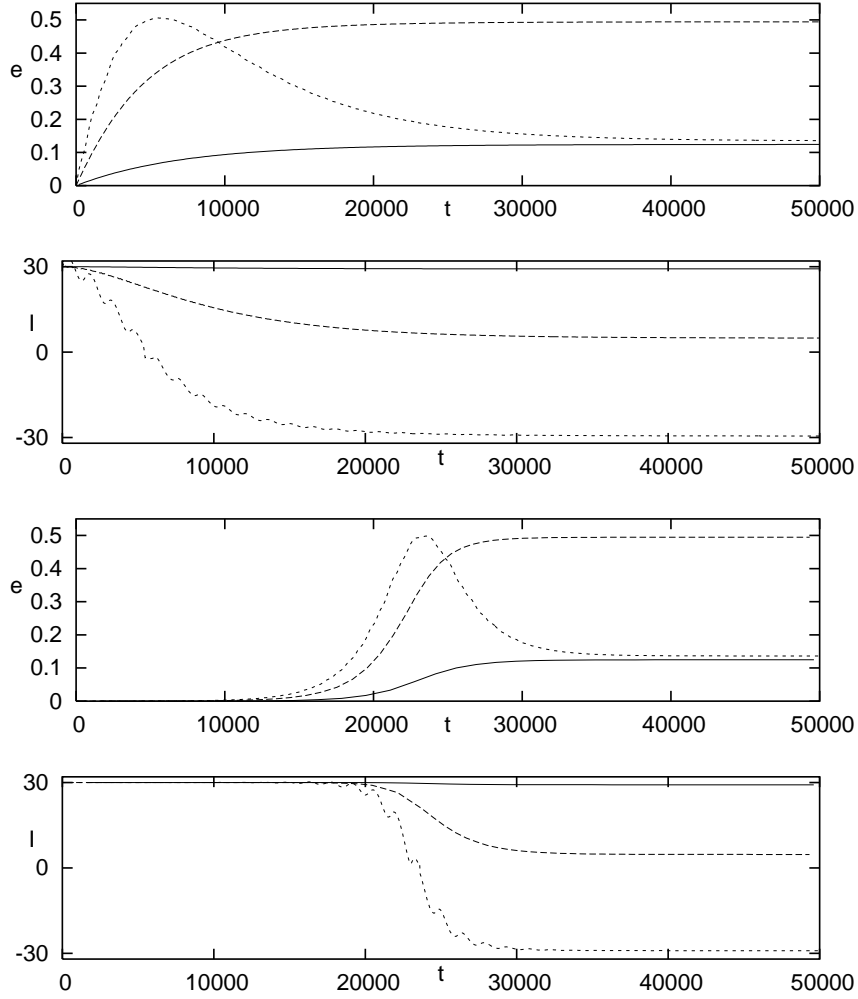


Fig. 3.— Eccentricity excitation by time-dependent constant-direction accelerations. The full equations of motion (2) are integrated numerically with the forms A_1 (two upper panels) and A_2 (two lower panels) and $I_0 = 30^\circ$. The parameters are: $A_0 = 2.21 \times 10^{-11} \text{ km s}^{-2}$ and $t_0 = 2.3 \times 10^4$ years. The oscillation period at 1 AU is 1.11×10^5 years. The timescale τ is chosen so that $V = 5 \text{ km s}^{-1}$; $\tau = 7200$ for A_1 and $\tau = 2300$ years for A_2 . The curves correspond the semi-major axes: 1 AU (solid), 32 AU (dashed) and 128 AU (dotted). Note how the final e and I are equal under the two different accelerations at each semi-major axis.

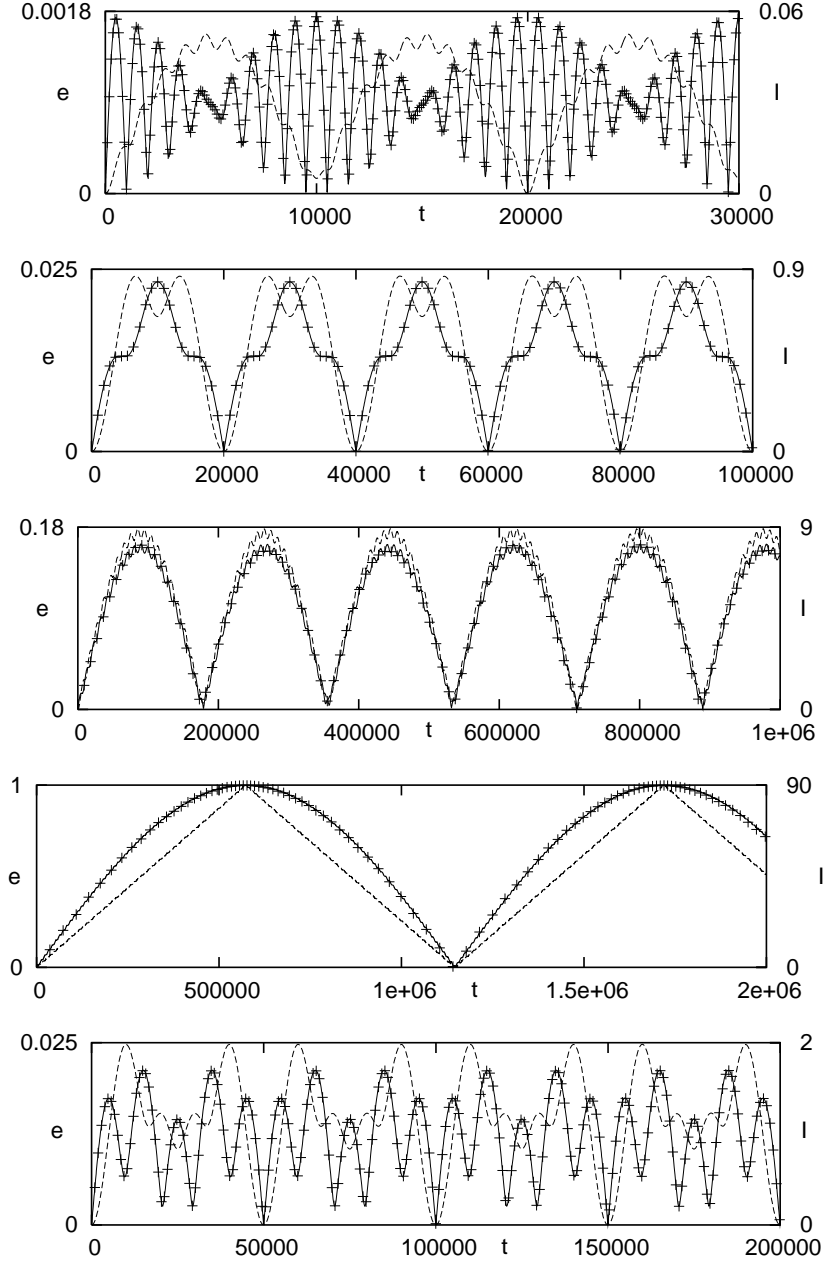


Fig. 4.— Excitation of the eccentricity (solid) and inclination (dashed) by a nearly perpendicular precessing jet with an angle $\alpha = 1^\circ$. The companion’s orbit is located at $a = 1$ AU and evolves from a circular orbit in a plane orthogonal to the jet’s precession axis. The acceleration is $A_0 = 2 \times 10^{-10} \text{ km s}^{-2}$ yielding an excitation time of $2\pi/n_A = 10^4$ years. From top to bottom, the panels were obtained from equations (23–24) with the frequency ratios, p : 0.05, 0.5, 0.9, 1 and 5 – the precession period is $2p \times 10^4$ years. The symbols correspond to the numerical integration of the full equations of motion (2) and show that the agreement with the averaged analytical solution is perfect.

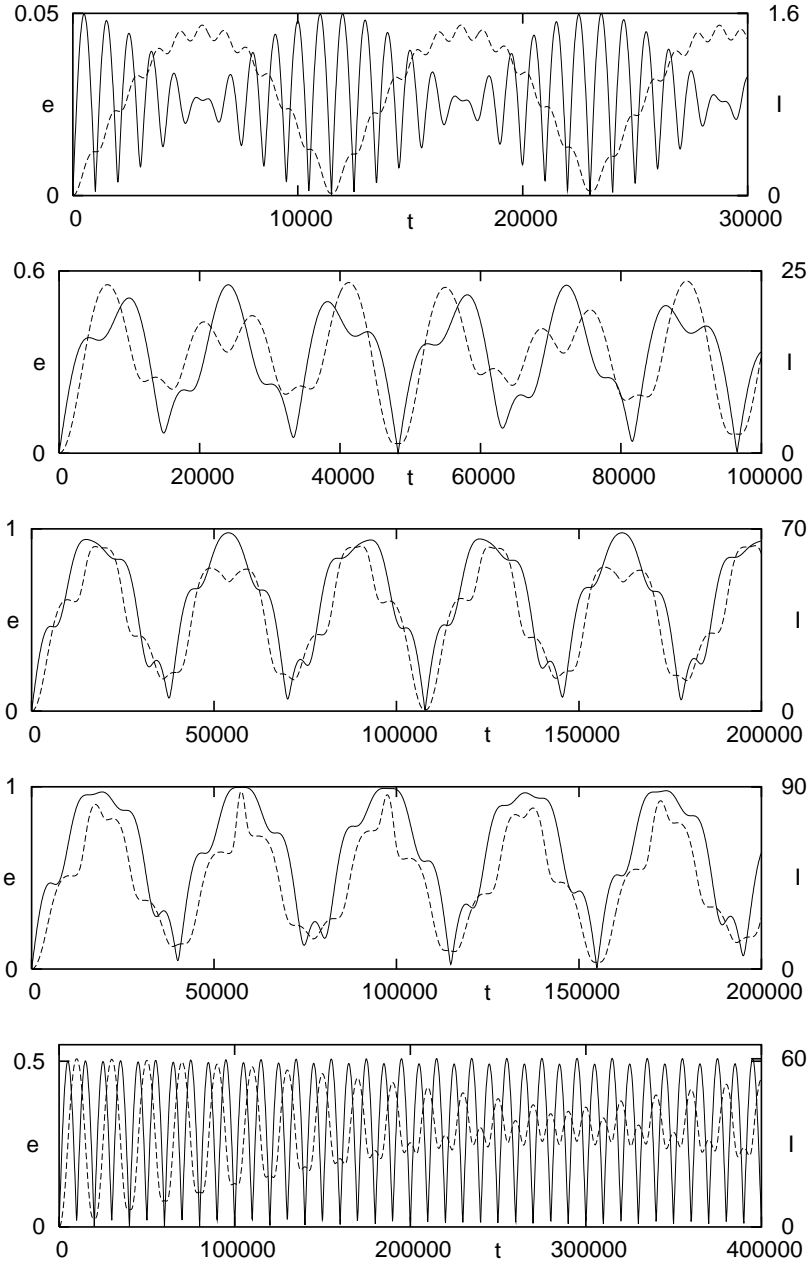


Fig. 5.— Same as Figure (4) for a jet angle $\alpha = 30^\circ$. From top to bottom, the panels correspond to the frequency ratios, p : 0.05, 0.5, 0.9, 1 and 50.

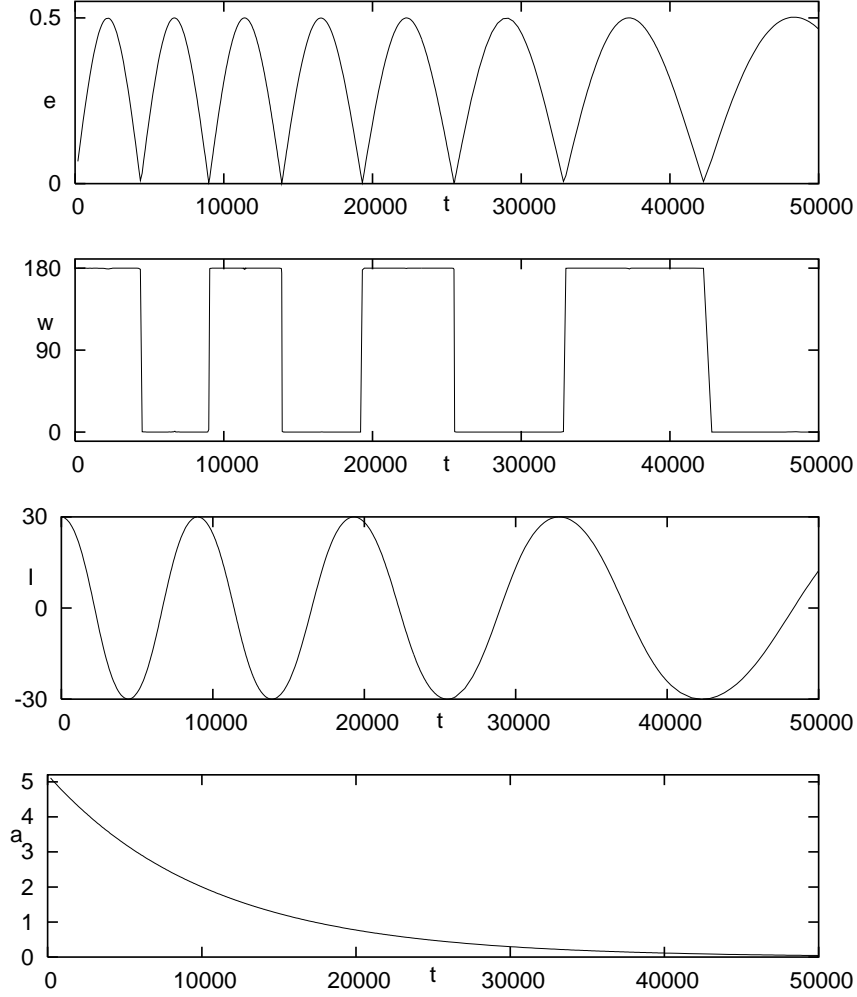


Fig. 6.— Effect of radial migration on eccentricity excitation. In this numerical integration of (2) with a constant direction acceleration of magnitude $A_0 = 2 \times 10^{-10} \text{ km s}^{-2}$ and inclination $I_0 = 30^\circ$, a Stokes drag term, $-k\mathbf{v}$ with $k^{-1} = 36\,500$ years, was added to the equations of motion. From top to bottom, the panels show the eccentricity, argument of pericenter, the inclination and the semi-major axis. The companion is located at 5.2 AU on an initially circular orbit. The initial excitation period is 4400 years. The slow migration with respect to the orbital motion affects the eccentricity evolution only through the oscillation period.

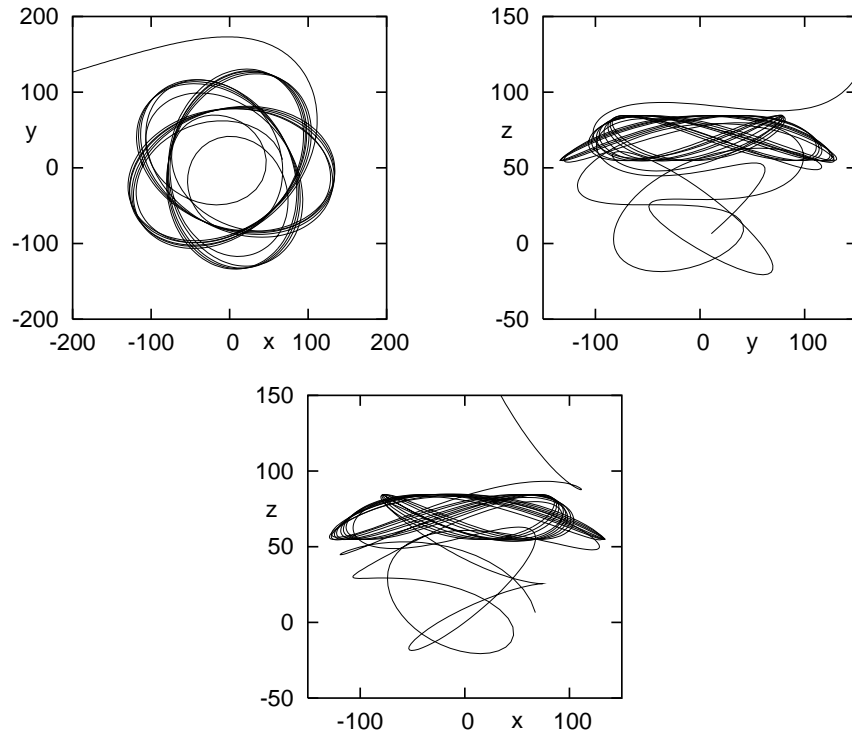


Fig. 7.— Escape of a companion located near the keplerian boundary of a conservative constant-direction acceleration with $I_0 = 30^\circ$. The distances are given in AU. The boundary’s semi-major axis is $a_{\text{kepler}} = 100 \text{ AU}$. Note how the companion hovers above the star before escaping. The corresponding orbital elements are shown in Figure (8).

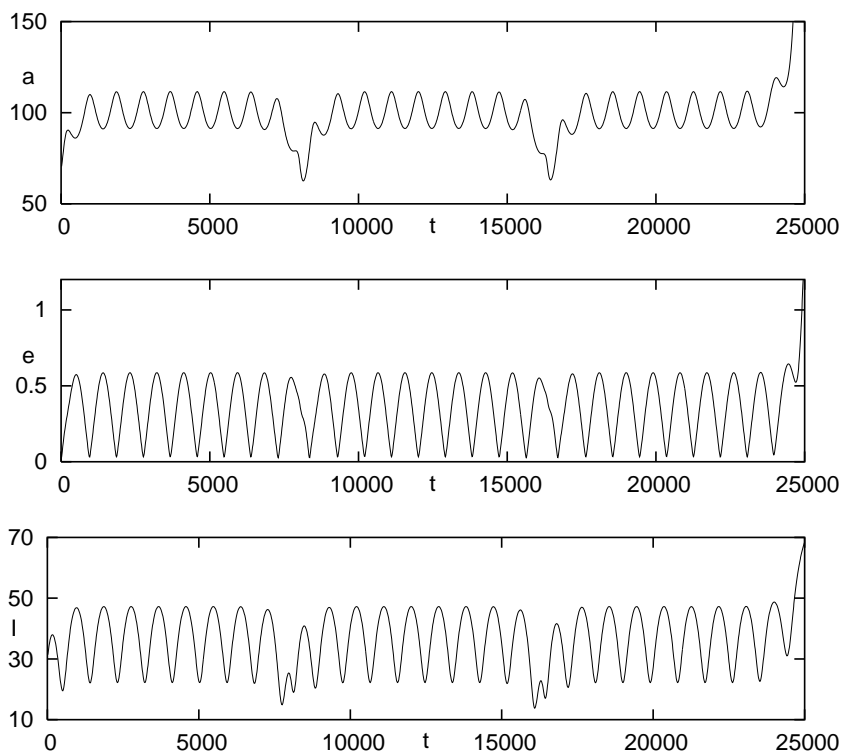


Fig. 8.— Escape of a companion located near the keplerian boundary of a conservative constant-direction acceleration. The boundary’s semi-major axis is $a_{\text{kplr}} = 100$ AU. The companion is initially on a circular orbit of semi-major axis 68.5 AU with $I_0 = 30^\circ$. The semi-major axis experiences large amplitude librations about a_{kplr} . The eccentricity amplitude is larger than $\sin I_0$ and the inclination evolution differs from that inside the keplerian region.

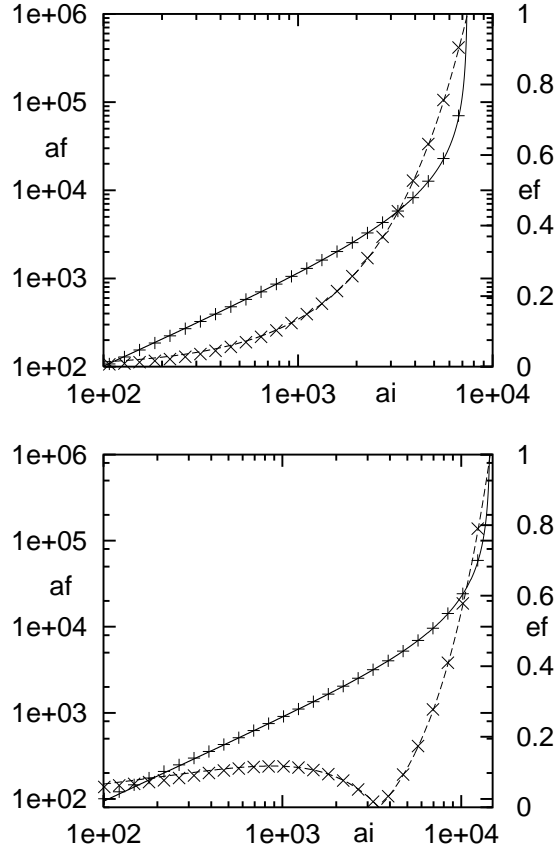


Fig. 9.— Migration and eccentricity excitation near the keplerian boundary of a finite duration acceleration for two inclination values $I_0 = 0$ (upper panel) and $I_0 = 20^\circ$ (lower panel). In each panel, the final semi-major axis a_f (AU) (solid) and the final eccentricity e_f (dashed) are shown as a function of the initial semi-major axis a_i (AU) as given by equations (29) and the numerical integration of the full equations of motion (2) (symbols). The parameters are: $V = 0.35 \text{ km s}^{-1}$, $a_{\text{kplr}} = 300 \text{ AU}$, and $\tau = 500 \text{ years}$. The inclined circular orbits were started at the descending node ($\theta = 180^\circ$). For $I_0 = 0^\circ$, $a_\infty = 7341 \text{ AU}$ and for $I_0 = 20^\circ$, $a_{\text{out}} = 3477 \text{ AU}$, $a_{\text{esc}} = 3797 \text{ AU}$, $a_\infty = 14542 \text{ AU}$.

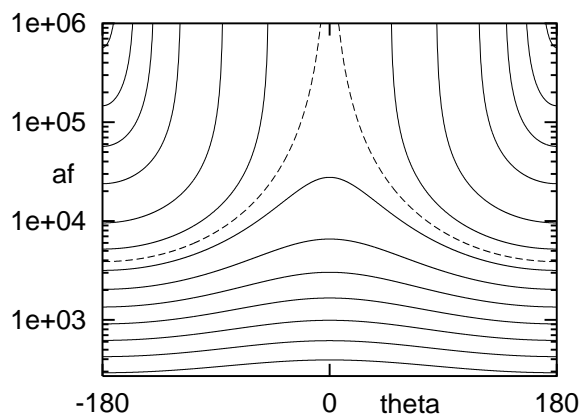


Fig. 10.— Final semi-major axes some of the initially inclined orbits ($I_0 = 20^\circ$) of Figure (9) as a function of orbital longitude θ . The dashed curve corresponds an initial semi-major axis at a_{esc} .

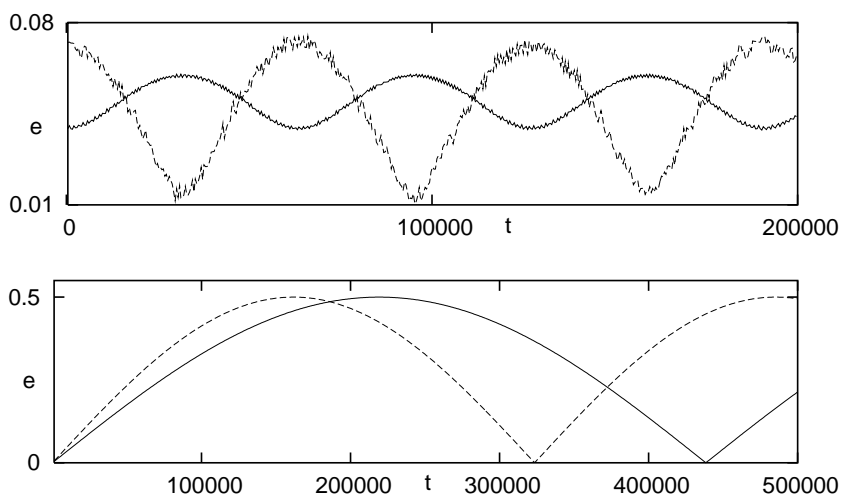


Fig. 11.— The evolution of the eccentricity of Jupiter (solid) and Saturn (dashed). In the top panel mutual interactions are included but no external acceleration is present. The planets' initial eccentricities are $e_J = 0.04$ and $e_S = 0.07$. In the bottom panel, an external acceleration with $a_{\text{kplr}} = 10^3$ AU acts on the two planets initially on circular coplanar orbits while mutual interactions are turned off.

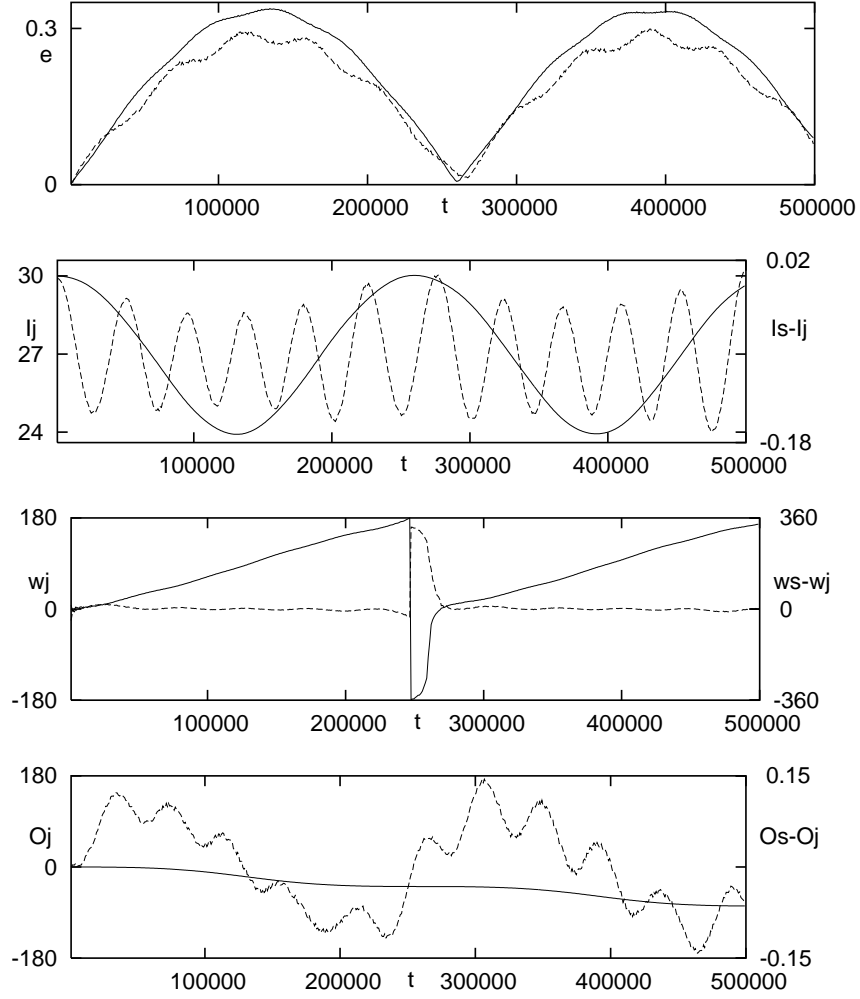


Fig. 12.— The excitation of Jupiter’s and Saturn’s eccentricities and inclinations by a constant-direction acceleration with $a_{\text{kplr}} = 10^3$ AU including the planets’ mutual gravitational interactions. The planets were started with circular co-planar orbits. From top to bottom, the panels show the evolution of the eccentricities, Jupiter’s inclination (solid) and the mutual inclination (dashed), Jupiter’s argument of perihelion (solid) and the mutual argument of perihelion (dashed), Jupiter’s longitude of ascending node (solid) and the mutual longitude of ascending node (dashed).

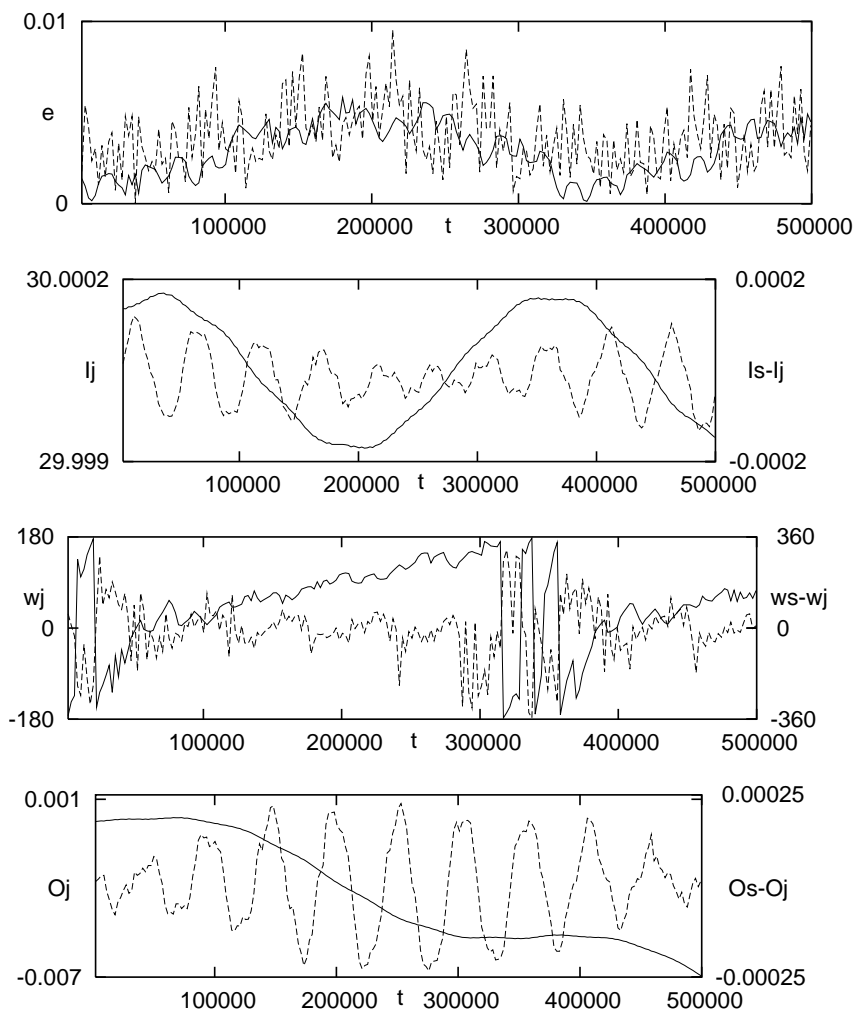


Fig. 13.— The excitation of Jupiter’s and Saturn’s eccentricities and inclinations by a constant direction acceleration with $a_{\text{kplr}} = 10^4$ AU including the planets’ mutual gravitational interactions. The planets were started with circular co-planar orbits. From top to bottom, the panels show the evolution of the eccentricities, Jupiter’s inclination (solid) and the mutual inclination (dashed), Jupiter’s argument of perihelion (solid) and the mutual argument of perihelion (dashed), Jupiter’s longitude of ascending node (solid) and the mutual longitude of ascending node (dashed).

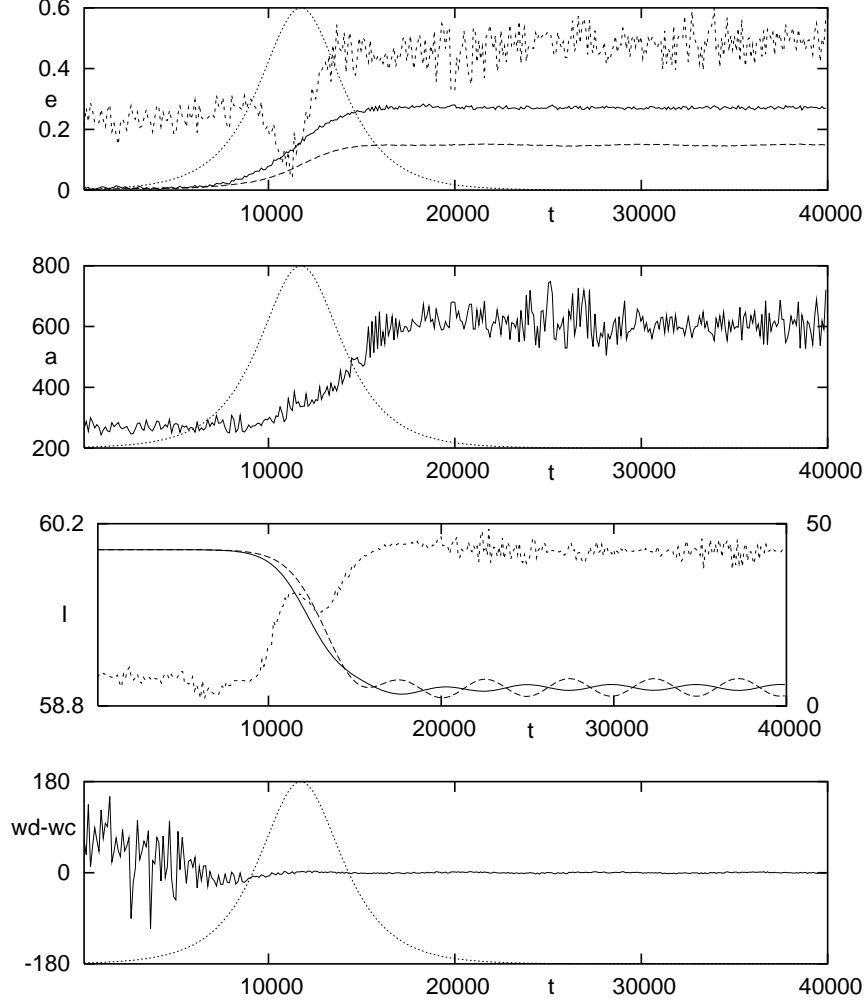


Fig. 14.— Eccentricity excitation, apsidal alignment and binary migration in the v And system. The acceleration is of the form A_2 (dotted) with $A_0 = 2.8 \times 10^{-11} \text{ km s}^{-2}$, $\tau = 2000$ years, $t_0 = 12000$ years corresponding to $a_{\text{kplr}} = 300$ AU and a residual velocity $V = 5.6 \text{ km s}^{-1}$. From the top down, The first panel shows the eccentricity excitation of planets d (solid) and c (dashed) and the eccentricity evolution of v And B (short-dashed) as well as the acceleration pulse normalized to its maximum value (dotted). The second panel shows the radial migration of v And B. The third panel shows the inclination of planets d (solid, left scale) and c (dashed, left scale) and the inclination evolution of v And B (short-dashed, right scale). The last panel shows the relative apsidal libration of planets d and c .